





RESEARCH PAPER

K_V1.3 channels are novel determinants of macrophage-dependent endothelial dysfunction in angiotensin II-induced hypertension in mice

Miguel A. Olivencia^{1,2,6}  | Marta Martínez-Casales^{1,3} | Diego A. Peraza⁴ | Ana B. García-Redondo^{1,5}  | Gema Mondéjar-Parreño^{2,6} | Raquel Hernanz^{3,5} | Mercedes Salaiques^{1,5} | Angel Cogolludo^{2,6}  | Michael W. Pennington⁷ | Carmen Valenzuela^{4,5} | Ana M. Briones^{1,5} 

¹Departamento de Farmacología, Universidad Autónoma de Madrid, Instituto de Investigación Hospital La Paz, Madrid, Spain

²Departamento de Farmacología y Toxicología, Facultad de Medicina, Universidad Complutense de Madrid, Instituto de Investigación Sanitaria Gregorio Marañón (IISGM), Madrid, Spain

³Departamento de Ciencias Básicas de la Salud, Facultad de Ciencias de la Salud, Universidad Rey Juan Carlos, Alcorcón, Spain

⁴Instituto de Investigaciones Biomédicas Alberto Sols (CSIC-UAM), Madrid, Spain

⁵Ciber de Enfermedades Cardiovasculares (CIBERCV), Spain

⁶Ciber de Enfermedades Respiratorias (CIBERES), Spain

⁷Peptides International Inc., Louisville, Kentucky, USA

Correspondence

Ana M. Briones, Departamento de Farmacología, Universidad Autónoma de Madrid, Instituto de Investigación Hospital La Paz, C/Arzobispo Morcillo 4, 28029, Madrid, Spain.
Email: ana.briones@uam.es

Carmen Valenzuela, Instituto de Investigaciones Biomédicas 'Alberto Sols' (CSIC-UAM), C/Arturo Duperier 4, 28029, Madrid, Spain.
Email: cvalenzuela@iib.uam.es

Present address

Ana B. García-Redondo, Departamento de

Background and Purpose: K_V1.3 channels are expressed in vascular smooth muscle cells (VSMCs), where they contribute to proliferation rather than contraction and participate in vascular remodelling. K_V1.3 channels are also expressed in macrophages, where they assemble with K_V1.5 channels (K_V1.3/K_V1.5), whose activation generates a K_V current. In macrophages, the K_V1.3/K_V1.5 ratio is increased by classical activation (M1). Whether these channels are involved in angiotensin II (AngII)-induced vascular remodelling, and whether they can modulate the macrophage phenotype in hypertension, remains unknown. We characterized the role of K_V1.3 channels in vascular damage in hypertension.

Experimental Approach: We used AngII-infused mice treated with two selective K_V1.3 channel inhibitors (HsTX[R14A] and [EWSS]ShK). Vascular function and structure were measured using wire and pressure myography, respectively. VSMC and macrophage electrophysiology were studied using the patch-clamp technique; gene expression was analysed using RT-PCR.

Key Results: AngII increased K_V1.3 channel expression in mice aorta and peritoneal macrophages which was abolished by HsTX[R14A] treatment. K_V1.3 inhibition did not prevent hypertension, vascular remodelling, or stiffness but corrected AngII-induced macrophage infiltration and endothelial dysfunction in the small mesenteric arteries and/or aorta, via a mechanism independent of electrophysiological changes in VSMCs. AngII modified the electrophysiological properties of peritoneal macrophages, indicating an M1-like activated state, with enhanced expression of proinflammatory cytokines that induced endothelial dysfunction. These effects were prevented by K_V1.3 blockade.

Abbreviations: [EWSS]ShK, mutant toxin present in the sea anemone *Stichodactyla helianthus*; AngII, angiotensin II; DEA-NO, diethylamine NONOate; EDHF, endothelium-derived hyperpolarizing factor; *E_m*, membrane potential; HsTX[R14A], mutant toxin present in the scorpion toxin HsTX1 from *Heterometrus spinnifer*; KHS, Krebs-Henseleit solution; M1, classical activation; M2, alternative activation; VSMCs, vascular smooth muscle cells.

Michael W. Pennington, AmbioPharm Inc., North Augusta, SC 29842, USA.

Miguel A. Olivencia, Marta Martínez-Casales and Diego A. Peraza contributed equally to this study.

Fisiología, Facultad de Medicina, Universidad Autónoma de Madrid, Madrid, Spain.

Funding information

Comunidad de Madrid-Universidad Autónoma de Madrid, Grant/Award Number: SI1-PJ1-2019-00321; European Commission; Comunidad de Madrid, Grant/Award Numbers: B2017/BMD-3727, B2017/BMD-3676-AORTASANA; Consejo Superior de Investigaciones Científicas, Grant/Award Numbers: 2019AEP148, 201820E104; Instituto de Salud Carlos III, Grant/Award Numbers: CB/11/00222, CB16/11/00286; Ministerio de Economía y Competitividad, Grant/Award Numbers: SAF2016-77222-R, SAF2016-80305-P, PID2019-104366RB-C21, SAF2016-75021-R

Conclusions and Implications: We unravelled a new role for $K_V1.3$ channels in the macrophage-dependent endothelial dysfunction induced by AngII in mice which might be due to modulation of macrophage phenotype.

KEYWORDS

angiotensin II, endothelial dysfunction, $K_V1.3$ channels, macrophages, vascular myocytes

1 | INTRODUCTION

Potassium channel activity is an important determinant of vascular tone by regulating membrane potential (E_m) in vascular smooth muscle cells (VSMCs). Activation of K^+ channels leads to membrane hyperpolarization, which results in reduced Ca^{2+} influx through L-type Ca^{2+} channels, and consequently, arterial relaxation, whereas their inhibition causes membrane depolarization and subsequent vasoconstriction (Cogolludo & Perez-Vizcaino, 2010; Jackson, 2018; Nelson & Quayle, 1995). Voltage-dependent potassium channels (K_V channels) are postulated to be major determinants of vascular tone (Jackson, 2018). Among them, the $K_V1.5$ channels are predominantly expressed in most conduit and resistance vessels, including portal vein, pulmonary arteries, renal arteries, aorta, and coronary arteries from rodents and humans (Clement-Chomienne et al., 1999; Cogolludo et al., 2006), and their impairment is associated with several cardiovascular diseases, such as hypertension, diabetes, and pulmonary hypertension (Jackson, 2018). In addition to $K_V1.5$ channels, $K_V1.3$ channels are also expressed in VSMCs, and experimental evidence suggests that they have a significant contribution in proliferation (Bobi et al., 2020; Ciudad et al., 2010; Perez-Garcia et al., 2018). In fact, the ratio of $K_V1.3/K_V1.5$ channel expression has been proposed as a marker of the VSMC phenotype (contractile/proliferative) (Perez-Garcia et al., 2018). Thus, it has been suggested that increased $K_V1.3$ and diminished $K_V1.5$ expression plays a role in vascular remodelling in different pathologies (Perez-Garcia et al., 2018). Whether these channels are involved in angiotensin II (AngII)-induced vascular remodelling and mechanical alterations remains unknown.

Macrophage functions depend on extracellular signal transduction. Some of these interactions involve changes in transmembrane ion fluxes that, in turn, modulate the network of intracellular signaling, that is, Ca^{2+} fluxes. Experimental evidence indicates that in macrophages, K_V currents are carried by heterotetrameric $K_V1.3/K_V1.5$ channels (Moreno et al., 2013; Vicente et al., 2006; Villalonga et al., 2010). Different stimuli may change the stoichiometry of these heterotetrameric K_V channels. Thus, proliferation and classical activation (M1) of macrophages increase the K_V current by (a) increasing the

What is already known

- $K_V1.3$ channels contribute to vascular smooth muscle cell proliferation and macrophage activation.

What this study adds

- $K_V1.3$ channel expression is increased in aorta and peritoneal macrophages from angiotensin II-induced hypertensive mice.
- $K_V1.3$ channel blockade prevents AngII-induced endothelial dysfunction and normalizes altered macrophage activation and vascular infiltration.

What is the clinical significance

- $K_V1.3$ blockers would be potentially attractive candidates for the treatment of autoimmune and vascular diseases.

$K_V1.3/K_V1.5$ ratio and/or (b) forming a certain degree of $K_V1.3$ homotetramers. However, alternative activation (M2) decreases the heterotetrameric channel ratio (Moreno et al., 2013; Villalonga et al., 2010). The activation of these macrophages may change the microenvironment and, thus, modify the functions of different tissues. The $K_V1.3$ channel is widely regarded as a therapeutic target for immunomodulation in autoimmune diseases. Thus, several $K_V1.3$ inhibitors are under development as therapeutic agents. Among them, there are synthetic analogues derived from the $K_V1.3$ -blocking peptide present in the sea anemone *Stichodactyla helianthus* toxin ([EWSS]ShK) and from the scorpion toxin *Heterometrus spinifer* (HsTX1) and its derivatives, such as HsTX[R14A]. Therefore, these peptides, which are highly selective $K_V1.3$ channel blockers, are potential candidates for the treatment of autoimmune diseases such as multiple sclerosis and

rheumatoid arthritis, and some of them are currently involved in clinical trials (Chang et al., 2015; Rashid et al., 2014; Tanner et al., 2017).

Consistent data indicate that cells from the innate and adaptive immune systems play a role in hypertension and hypertension-associated target organ damage by infiltrating vessels, kidneys, heart, and brain where they produce various proinflammatory cytokines and chemokines (Caillon et al., 2019; Drummond et al., 2019; Norlander et al., 2018). At the vascular level, this low-grade inflammatory milieu facilitates increased oxidative stress and decreased NO bioavailability, which leads to vasoconstriction and endothelial dysfunction, and increases collagen synthesis resulting in stiffening of the vessels and remodelling (Caillon et al., 2019; Drummond et al., 2019; Norlander et al., 2018). Specifically, enhanced macrophage infiltration has been found in several models of hypertension including that induced by infusion of angiotensin II (AngII) in mice (reviewed in Caillon et al., 2019; Drummond et al., 2019; Norlander et al., 2018). Moreover, a causal role for monocytes and macrophages in the development of hypertension, vascular remodelling, and endothelial dysfunction has been previously shown (De Ciuceis et al., 2005; Ko et al., 2007; Kossmann et al., 2014; Wenzel et al., 2011). However, the role of $K_V1.3$ channels in macrophages in hypertension-associated vascular damage is unknown.

The aim of this study was to characterize the role of $K_V1.3$ channels in vascular damage in hypertension. We used selective inhibitors of $K_V1.3$ channels to evaluate VSMC and macrophage electrophysiology, vascular function and remodelling, and macrophage phenotype.

2 | METHODS

2.1 | Animal models

2.1.1 All animal care and experimental procedures were approved by the Ethical Committee of Research of the Universidad Autónoma de Madrid and Dirección General de Medio Ambiente, Comunidad de Madrid, Spain (PROEX 345/14). Animals were taken care of and used according to the Spanish Policy for Animal Protection RD53/2013, which meets the European Union Directive 2010/63/UE on the protection of animals used for experimental and other scientific purposes. The experiments were conducted in accordance with the National Institutes of Health (NIH) Guide for the Care and Use of Laboratory Animals. Animal studies are reported in compliance with the ARRIVE guidelines (Percie du Sert et al., 2020) and with the recommendations made by the *British Journal of Pharmacology* (Lilley et al., 2020). The animal studies complied with the 3Rs.

All mice were bred at the conventional Animal Care Facility of the Faculty of Medicine, Universidad Autónoma de Madrid (UAM) under controlled conditions at 25°C in a 12-h light/dark cycle, with ad libitum access to water and food. Animals were housed in groups of three to four in standard polypropylene cages containing rich bedding made of dried wood chips.

Alzet osmotic minipumps (Alza Corp., Cupertino, CA, USA; 2002 model), delivering AngII (1.44 mg·kg⁻¹·day⁻¹) were implanted

subcutaneously for 2 weeks into 3-month-old male C57BL6/J mice (weight 25–30 g). For the implantation of osmotic minipumps, the mice were anaesthetized with isoflurane inhalation (2%). Anaesthetic depth was confirmed by loss of blink reflex and/or lack of response to tail pinch. The procedure took approximately 15 min per mouse. Recovery after surgical procedures was performed using aseptic techniques in a dedicated approved surgical area. Analgesics (buprenorphine, 0.05 mg·kg⁻¹, s.c.) were administered immediately after surgery to prevent discomfort. The animals were kept warm in a heating pad until awake after surgery and observed carefully by the investigators throughout the post-surgery period.

The selective $K_V1.3$ channel inhibitors HsTX[R14A] and [EWSS] ShK (Chang et al., 2015; Rashid et al., 2014) or the solvent were injected subcutaneously into control and AngII-treated mice (100 µg·kg⁻¹ per injection), every second day for 15 days, starting the day before AngII infusion, according to previous studies (Bergmann et al., 2017; Upadhyay et al., 2013). BP was measured using tail-cuff plethysmography. The animals were trained by observers, who were unaware of the vascular experiments for 1 week prior to the final BP measurements. Measurements were always performed at the same time of the day. Five individual observations were performed and averaged for each animal.

Male AngII-infused mice were used, as this is a good model for hypertension that resembles some forms of human hypertension (Lerman et al., 2019), without interference from the effects of female hormones or the oestrous cycle. Animals were randomly distributed in the different experimental groups with each group having the same number of animals by design. The mice were labelled by an operator unaware of the nature of the experiments. We did not utilize statistical methods to predetermine sample or group sizes, and the number of animals used was estimated from our previous experience with this animal model. Investigators for outcome assessments were not blinded to group allocation.

2.1.1 | Tissue preparation and isolation of intraperitoneal macrophages

The mice were killed with CO₂. Aorta, perivascular adipose tissue, and first-order branches of the mesenteric artery were removed and placed in cold (4°C) Krebs–Henseleit solution (KHS) with the following composition (in mmol·L⁻¹): 115 NaCl, 25 NaHCO₃, 4.7 KCl, 1.2 MgSO₄·7H₂O, 2.5 CaCl₂, 1.2 KH₂PO₄, 11.1 glucose, and 0.01 Na₂EDTA, bubbled with a 95% O₂–5% CO₂ mixture (pH = 7.4).

Intraperitoneal macrophages from control, AngII, AngII + [EWSS] ShK, and AngII + HsTX[R14A] mice were obtained in PBS (Khemili et al., 2019; Zhang et al., 2008) and cultured in DMEM, supplemented with 10% FBS, 100 IU·ml⁻¹ penicillin, 100 µg·ml⁻¹ streptomycin, and 10 mmol·L⁻¹ L-glutamine, for 24 h. Macrophage-conditioned media were collected and stored at –80°C. The mRNA and protein from macrophages were obtained and quantified.

Vascular function, structure, and mechanics were analysed on the same day. Other vascular segments were immediately frozen in liquid nitrogen and stored at -70°C until further processing for gene expression.

2.2 | Quantitative RT-PCR assay

The different mRNAs were determined in mouse aortic segments (containing adventitial cells, VSMCs, and endothelial cells), perivascular adipose tissue, or macrophages by qRT-PCR. Total RNA was extracted using TRI Reagent according to the manufacturer's recommendations. A total of $1\ \mu\text{g}$ of RNA was reverse-transcribed into cDNA using a High-Capacity cDNA Archive Kit (Invitrogen Life Technologies) with random hexamers. qPCR was performed in a 7500 Fast ABI System (Invitrogen Life Technologies) using commercial mouse primers (Table S1).

PCR cycle programs were as follows: initial denaturation for 30 s at 95°C , followed by 40 cycles at 95°C for 5 s, and 60°C for 30 s. Melting curve analysis was performed in SYBR green reactions to show PCR product specificity. To ensure the reliability of the qRT-PCR values, samples were analysed in duplicate. Data analysis and data presentation were performed using the average of the duplicated values of each sample. To calculate the relative index of gene expression, we employed the $2^{-\Delta\Delta\text{Ct}}$ method, where β_2 -microglobulin served as the internal control, using untreated samples from control mice as the calibrator. Thus, the PCR data were normalized to the mean values of the control group to minimize variation.

2.3 | Pressure myography

The structural and mechanical properties of the small mesenteric arteries were studied using a pressure myograph (Danish Myo Tech, Model P100, J.P. Trading I/S, Aarhus, Denmark) as previously described (Briones et al., 2003). Vessels were placed on two glass microcannulae and secured with surgical nylon sutures. After each small branch was tied off, the vessel length was adjusted so that the vessel walls were parallel without stretching. Intraluminal pressure was subsequently raised to 120 mmHg, and the artery was unbuckled by adjusting the cannulae. The segment was then set to a pressure of 45 mmHg and allowed to equilibrate for 30 min at 37°C in calcium-free KHS (0Ca^{2+} ; omitting calcium and adding $1\ \text{mmol}\cdot\text{L}^{-1}$ EGTA) with intravascular and extravascular perfusion, gassed with a mixture of 95% O_2 and 5% CO_2 . Intraluminal pressure was reduced to 3 mmHg. A pressure-diameter curve was obtained by increasing intraluminal pressure in 20 mmHg steps from 3 to 120 mmHg. Internal and external diameters ($D_{i\text{OCa}}$, $D_{e\text{OCa}}$) were continuously measured under passive conditions for 3 min at each intraluminal pressure. The final value used was the mean of the measurements taken during the last 30 s when the measurements reached a steady state.

2.3.1 | Calculation of passive structural and mechanical parameters

From internal and external diameter measurements in passive conditions, the following structural and mechanical parameters were calculated:

$$\text{Wall thickness (WT)} = (D_{e\text{OCa}} - D_{i\text{OCa}}) / 2,$$

$$\text{Wall : lumen} = (D_{e\text{OCa}} - D_{i\text{OCa}}) / 2D_{i\text{OCa}}.$$

Circumferential wall strain (ϵ) = $(D_{i\text{OCa}} - D_{0\text{OCa}}) / D_{0\text{OCa}}$, where $D_{0\text{OCa}}$ is the internal diameter at 3 mmHg and $D_{i\text{OCa}}$ is the observed internal diameter for a given intravascular pressure both measured in 0Ca^{2+} medium.

Circumferential wall stress (σ) = $(P \times D_{i\text{OCa}}) / (2\text{WT})$, where P is the intraluminal pressure ($1\ \text{mmHg} = 1.334 \times 10^3\ \text{dynes}\cdot\text{cm}^{-2}$) and WT is the wall thickness at each intraluminal pressure in 0Ca^{2+} -KHS.

The arterial stiffness independent of the geometry was determined by the Young's elastic modulus ($E = \text{stress}/\text{strain}$). The stress-strain relationship is non-linear; therefore, it is more appropriate to obtain a tangential or incremental elastic modulus (E_{inc}) by determining the slope of the stress-strain curve ($E_{\text{inc}} = \delta\sigma / \delta\epsilon$). E_{inc} was obtained by fitting the stress-strain data from each animal to an exponential curve using the equation: $\sigma = \sigma_{\text{orig}} e^{\beta\epsilon}$, where σ_{orig} is the stress at the original diameter (diameter at 3 mmHg). Taking derivatives of the equation, we determined that $E_{\text{inc}} = \beta\sigma$. For a given σ -value, E_{inc} is directly proportional to β . An increase in β implies an increase in E_{inc} , which indicates an increase in stiffness.

2.4 | Aortic wall thickness

OCT-embedded aortic sections were stained with the nuclear dye DAPI (Thermo Fisher Scientific) for 10 min followed by washing with PBS. The media thickness of each aorta was measured using ImageJ software (NIH, Bethesda, MD, USA).

2.5 | Wire myography

Reactivity of the mouse aorta and small mesenteric arteries was studied using a wire myograph. After a 30-min equilibration period in oxygenated KHS, arterial segments were stretched to their optimal lumen diameter for active tension development. Contractility of the segments was then tested by an initial exposure to a high- K^+ solution (K^+ -KHS, $120\ \text{mmol}\cdot\text{L}^{-1}$). The presence of endothelium was determined by the ability of $10\ \mu\text{mol}\cdot\text{L}^{-1}$ ACh to relax arteries precontracted with phenylephrine at approximately 50% of K^+ -KHS contraction. Arteries were discarded if K^+ -KHS response was $\leq 0.5\ \text{mN}\cdot\text{mm}^{-1}$ or relaxed $\leq 20\%$ to ACh. Next, a single concentration-response curve to ACh ($1\ \text{nmol}\cdot\text{L}^{-1}$ to $30\ \mu\text{mol}\cdot\text{L}^{-1}$) and the NO donor diethylamine NONOate (DEA-NO, $1\ \text{nmol}\cdot\text{L}^{-1}$ to

30 $\mu\text{mol}\cdot\text{L}^{-1}$) was obtained for phenylephrine or **U46619** precontracted aorta and mesenteric arteries, respectively.

In another set of experiments, we investigated the involvement of endothelium-derived hyperpolarizing factor (EDHF) in the ACh-induced responses of small mesenteric arteries in control, AngII, and AngII + HsTX[R14A] mice. For this, we incubated the segments with a combination of a non-selective NOS inhibitor nitro-L-arginine methyl ester (L-NAME, 100 $\mu\text{mol}\cdot\text{L}^{-1}$) and a non-selective cyclooxygenase (COX) inhibitor **indomethacin** (10 $\mu\text{mol}\cdot\text{L}^{-1}$) for 30 min, so that the remaining vasodilator response could be attributed to EDHF. Next, a concentration–response curve to ACh was obtained in U46619 precontracted arteries.

To minimize variation, vasodilator responses were expressed as a percentage of the previous tone induced by phenylephrine or U46619 in each case.

2.6 | Endothelial cell culture

Human microvascular endothelial cells (HMEC-1, ATCC®, Middlesex, UK; CRL-3243™, RRID:CVCL_0307) were cultured according to the manufacturer's instructions. At 80% confluence, the cells were serum-deprived for 24 h before stimulation. Then endothelial cells were stimulated with AngII (1 $\text{nmol}\cdot\text{L}^{-1}$ for 6 and 24 h). Control cells were stimulated with vehicle. RNA was isolated, and qRT-PCR experiments were performed as described above.

2.7 | Electrophysiology of VSMCs and peritoneal macrophages

VSMCs from mouse aorta were isolated by enzymatic digestion as previously described (Briones, Padilha, et al., 2009), and peritoneal macrophages were obtained as stated above. In both cell types, membrane currents were recorded with an Axopatch 200B and a Digidata 1322A (Axon Instruments, Burlingame, CA, USA) using the whole-cell configuration of the patch-clamp technique. VSMCs were superfused with an (external) Ca^{2+} -free HEPES solution with the following composition (in $\text{mmol}\cdot\text{L}^{-1}$): 130 NaCl, 5 KCl, 1.2 MgCl_2 , 10 glucose, and 10 HEPES (pH 7.3 with NaOH) and a Ca^{2+} -free pipette (internal) solution containing ($\text{mmol}\cdot\text{L}^{-1}$): 130 KCl, 1.2 MgCl_2 , 5 Na_2ATP , 10 HEPES, and 10 EGTA (pH adjusted to 7.3 with KOH). Peritoneal macrophages were superfused with an external solution (in $\text{mmol}\cdot\text{L}^{-1}$): 130 NaCl, 4 KCl, 1.8 CaCl_2 , 1 MgCl_2 , 10 HEPES, and 10 glucose (pH 7.40 with NaOH) and a Ca^{2+} -free pipette (internal) solution containing ($\text{mmol}\cdot\text{L}^{-1}$): 80 K-aspartate, 50 KCl, 3 phosphocreatine, 10 KH_2PO_4 , 3 MgATP , 10 HEPES, and 5 EGTA (pH 7.25 with KOH), as previously described (Moreno et al., 2013).

K_V currents were evoked following the application of 200- or 250-ms depolarizing pulses from -60 to $+20$ mV in 10-mV increments in VSMCs or from -80 to $+60$ mV in 10-mV increments in macrophages. To characterize the contribution of $K_V1.3$ channels to the total K_V current in VSMCs, cells were exposed to the

selective inhibitor HsTX[R14A] (0.1 $\text{nmol}\cdot\text{L}^{-1}$). Currents were normalized for cell capacitance and expressed in $\text{pA}\cdot\text{pF}^{-1}$. Membrane potential was recorded under the current-clamp mode. All experiments were performed at room temperature (22–24°C). To analyse the electrophysiological effects of lipopolysaccharide (LPS), peritoneal macrophages were incubated with LPS (100 $\text{ng}\cdot\text{ml}^{-1}$) for 16 h. After this, macrophages were removed from the plates and used during the next 8 h. In another set of experiments, the acute effects of AngII (0.1 $\mu\text{mol}\cdot\text{L}^{-1}$) were studied, applying the protocols described above. After obtaining the control records, macrophages were perfused with an external solution containing AngII (0.1 $\mu\text{mol}\cdot\text{L}^{-1}$), and the same protocol was applied. We also performed a set of experiments to confirm that the K_V recorded in peritoneal macrophages from AngII-treated mice was mostly due to the activation of $K_V1.3$ homotetramers or $K_V1.3/K_V1.5$ heterotetramers with a high proportion of $K_V1.3$. Thus, we performed in vitro incubation of macrophages from AngII-infused mice with [EWSS]ShK (1 $\text{nmol}\cdot\text{L}^{-1}$) or HsTX[R14A] (0.1 $\text{nmol}\cdot\text{L}^{-1}$). OriginPro 2018 (OriginLab Co.) and the Clampfit utility of pClamp10 (RRID:SCR_011323) were used to perform least-squares fitting and data presentation. To minimize variation of the use-dependent decay observed during the application of trains of depolarizing pulses, the peak current of each trace was expressed versus the peak current generated after applying the first depolarizing pulse of each train in macrophages.

2.8 | Immunocytochemistry of $K_V1.3$ channels in peritoneal macrophages

The Immuno-related procedures used comply with the recommendations made by the *British Journal of Pharmacology* (Alexander et al., 2018). Peritoneal macrophages were seeded in 24-well multi-well plates, in which a sterile circular glass coverslip had been placed previously. The next steps of the protocol were carried out in a humid chamber and between each step; the preparations were washed with PBS. Macrophages were incubated with rabbit IgG polyclonal anti $K_V1.3$ (extracellular) antibody (1:150, APC-101, Alomone, RRID:AB_2040149) for 24 h at 4°C. The primary antibody was diluted in DMEM without serum or antibiotics. The cells were fixed in 4% paraformaldehyde for 20 min at room temperature. A blocking solution composed of PBS with 10% FBS (Gibco) was used for 45 min at room temperature to reduce non-specific reactions. The goat Alexa 546 anti-rabbit IgG polyclonal antibody (1:500, A11035, Thermo Fisher Scientific, RRID:AB_2534093) was used as the secondary antibody for 1 h at room temperature; the nuclear staining reagent **DAPI** (1:1,000) was used for 5 min at room temperature. Both the secondary antibody and DAPI were diluted in the blocking solution. Coverslips were mounted using ProLong Live Antifade Reagent (Thermo Fisher Scientific), examined using an LSM710 spectral confocal microscope (Zeiss), and processed using ZEN2009 image acquisition (Zeiss). When the incubation step with the anti- $K_V1.3$ antibody was omitted, no signal was detected, supporting the specificity of the primary

antibody (negative control experiments). In addition, LPS-polarized macrophages well known to express $K_v1.3$ channels were used as positive controls; their plasma membranes were successfully immunostained with this anti- $K_v1.3$ antibody (positive control experiments) (not shown). Fluorescence intensity was quantified using ImageJ software (NIH, RRID:SCR_001935) without being blinded to the group assignment.

2.9 | Ex vivo incubation of aortic segments with macrophage-conditioned media

Healthy aortic segments from C57BL6/J mice were exposed to macrophage-conditioned media for 20 h. The media were normalized to total macrophage protein content. In some experiments, arteries were co-incubated with the **IL-1 β** antagonist **anakinra** (100 $\mu\text{g}\cdot\text{mL}^{-1}$) or the selective **COX-2** inhibitor **celecoxib** (1 $\mu\text{mol}\cdot\text{L}^{-1}$) in the presence of AngII macrophage-conditioned media. Concentration-response curves to **ACh** and DEA-NO were obtained for each segment as described above.

2.10 | Data and statistical analysis

The data and statistical analysis comply with the recommendations of the *British Journal of Pharmacology* on experimental design and analysis in pharmacology (Curtis et al., 2018). Statistical analysis of the animal studies and VSMC electrophysiology was performed using GraphPad Prism Software (v7.04, RRID:SCR_002798). Statistical analysis of the electrophysiological studies in macrophages was performed using SPSS (v. 25, RRID:SCR_002865). All data are expressed as the mean \pm SEM. The number of biological replicates (n) is mentioned in the respective figure legends or graphs. The declared group size is the number of these biological replicates, and statistical analysis was performed using these independent values. Statistical analysis was undertaken only for studies in which each group size was at least $n = 5$. In some cases, group sizes became unequal during the study owing to biological loss (i.e., death of the mouse), technical failure, or presence of outliers that were excluded using predefined criteria. Shapiro-Wilk normality test was used to analyse the data distribution. Results were analysed using the Mann-Whitney non-parametric test or the Student's t test where appropriate (two-tailed), and one-way or two-way ANOVA followed by Bonferroni's or Tukey's post hoc test. Adjusted Bonferroni's multiple comparison post hoc tests were run when F achieved $P < 0.05$ and there was no significant variance in homogeneity. The ROUT method using GraphPad Prism software was used to exclude data from the analysis. P values < 0.05 were considered significant.

2.11 | Materials

Unless specified otherwise, drugs and general reagents were obtained from Sigma-Aldrich (Madrid, Spain). HsTX[R14A] and [EWSS]ShK

were kindly provided by Peptides International, Inc.; celecoxib was generously provided by Pfizer Inc.; anakinra was purchased from SOBI (Madrid, Spain).

All drugs were dissolved in water, except HsTX[R14A] and [EWSS]ShK which were dissolved in P6N buffer (NaHPO_4 10 $\text{mmol}\cdot\text{L}^{-1}$, NaCl 0.8%, Tween-20 0.05%, pH 6.0) and celecoxib which was dissolved in DMSO. Further dilutions were performed using distilled water.

2.12 | Nomenclature of targets and ligands

Key protein targets and ligands in this article are hyperlinked to corresponding entries in the IUPHAR/BPS Guide to PHARMACOLOGY (<http://www.guidetopharmacology.org>) and are permanently archived in the Concise Guide to PHARMACOLOGY 2019/20 (Alexander, Fabbro et al., 2019; Alexander, Mathie et al., 2019).

3 | RESULTS

3.1 | AngII increases expression of vascular $K_v1.3$ channels: contribution of $K_v1.3$ channels to vascular remodelling and stiffness

Two weeks of AngII infusion increased aortic *Kcna3* mRNA expression, which was abolished by HsTX[R14A] treatment (Figure 1a). *Kcna5* expression tended to increase after AngII and was not modified by HsTX[R14A] treatment (Figure 1a). We then tested the role of $K_v1.3$ channels in AngII-induced vascular remodelling and mechanical alterations by co-treating AngII-infused mice with two highly selective $K_v1.3$ blockers, HsTX[R14A] and [EWSS]ShK (Chang et al., 2015; Rashid et al., 2014). As shown in Figure 1b, HsTX[R14A] did not modify AngII-induced hypertension. As expected, AngII induced aortic hypertrophy (Figure 1c) and inward remodelling of small mesenteric arteries (indicated by decreased lumen diameter and increased wall thickness and wall:lumen ratio) and increased vascular stiffness (indicated by diminished strain, leftwardshift of stress-strain relationship and increased β value) (Figure 1d,e). These changes were not affected by HsTX[R14A] treatment (Figure 1c-e). Similarly, [EWSS]ShK treatment did not modify AngII-induced hypertension or vascular remodelling and stiffness (Figure S1). Neither HsTX[R14A] nor [EWSS]ShK altered BP or vascular *Kcna3* and *Kcna5* expression in control mice (data not shown).

3.2 | Blockade of $K_v1.3$ channels improves endothelial function in AngII-infused mice

As expected, AngII infusion impaired endothelium-dependent relaxation induced by ACh in both aorta and small mesenteric arteries, but it did not modify endothelium-independent relaxation to the NO donor DEA-NO (Figure 2a,b, Tables 1 and 2). Interestingly,

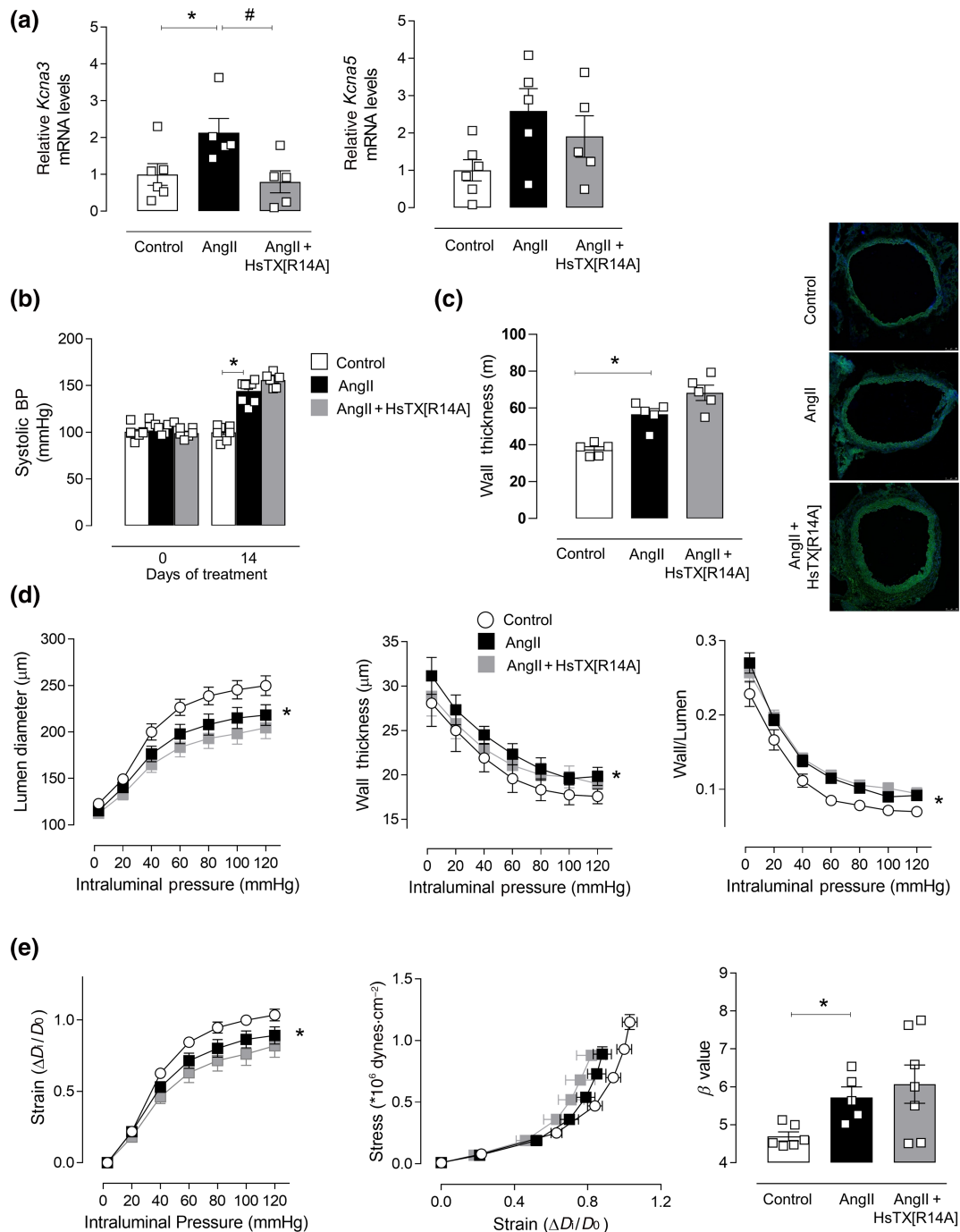


FIGURE 1 AngII-induced vascular remodelling and stiffness are not dependent on increased expression of $K_v1.3$ channels. (a) *Kcna3* and *Kcna5* mRNA expression in aorta from control ($n = 6$), AngII-infused ($n = 5$), and AngII + HsTX[R14A]-infused ($n = 5$) mice. (b) Systolic BP of control ($n = 8$), AngII-infused ($n = 7$), and AngII + HsTX[R14A]-infused ($n = 6$) mice. (c) Representative images (image size $1,055 \times 1,055 \mu\text{m}$) and quantification of aortic wall thickness of control, AngII- and AngII + HsTX[R14A]-treated animals ($n = 5$ all groups). (d) Structural and (e) mechanical parameters in small mesenteric arteries from control ($n = 6$), AngII-treated ($n = 6$), and AngII + HsTX[R14A]-treated ($n = 7$) animals. Results are presented as means \pm SEM. * $P < .05$, significantly different from control; # $P < .05$, significantly different from AngII; one-way (a,b,c,e) or two-way (d,e) ANOVA followed by Bonferroni's post hoc test

treatment with selective $K_v1.3$ channel blockers (HsTX[R14A] or [EWSS]ShK) prevented AngII-induced endothelial dysfunction in the aorta without modifications of endothelium-independent relaxation (Figures 2a and S2A, Tables 1 and 2), excluding augmented VSMC NO sensitivity as an underlying mechanism to explain the improved

endothelial function. HsTX[R14A] also improved endothelium-dependent relaxation in the small mesenteric arteries without modifying the endothelium-independent relaxation (Figure 2b, Table 1). The endothelium-dependent vasodilator **bradykinin** induced concentration-dependent relaxation in the small mesenteric arteries but not

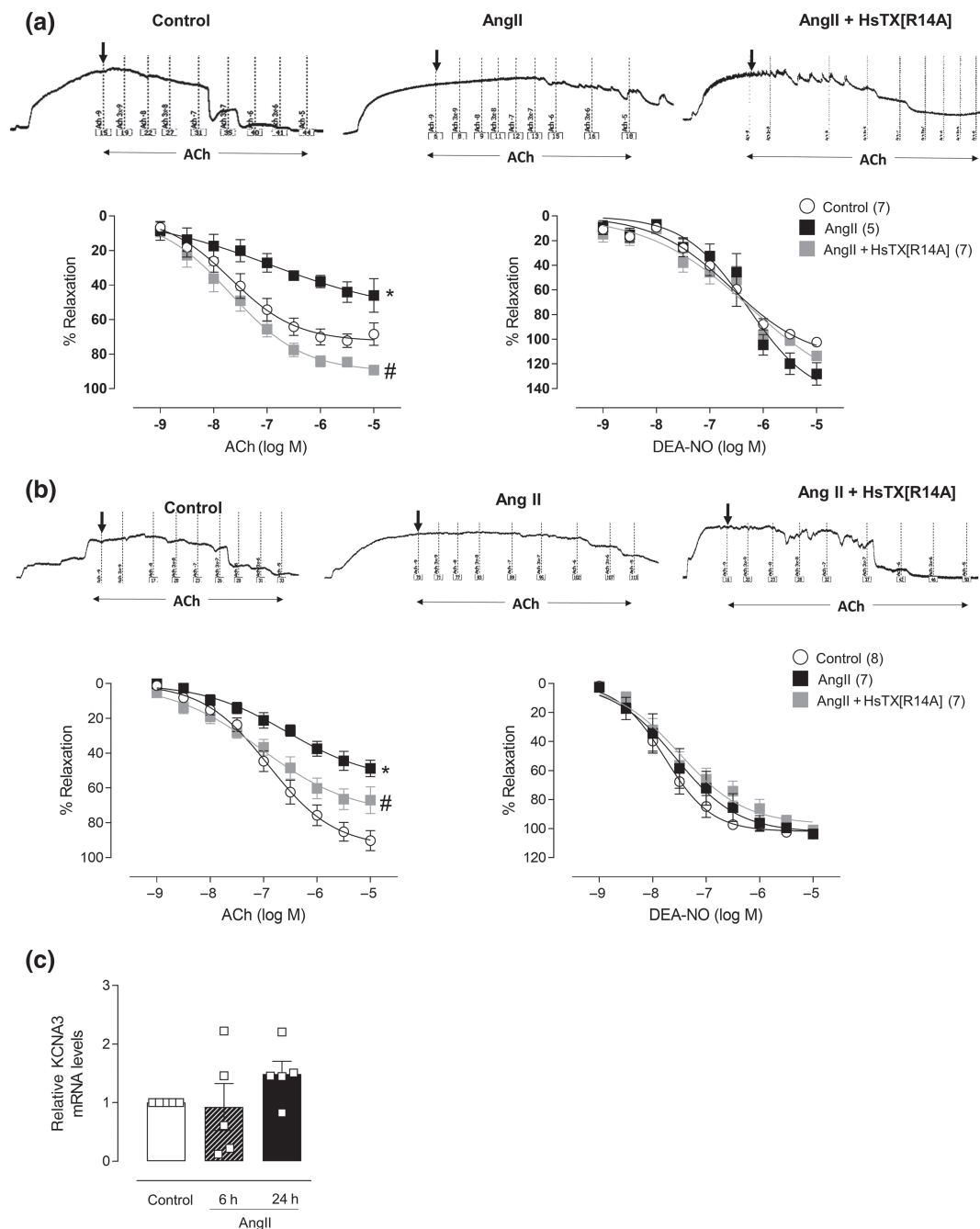


FIGURE 2 Blockade of $K_{v1.3}$ channels corrects AngII-induced endothelial dysfunction. Concentration–response curves to ACh and diethylamine NONOate (DEA-NO) in (a) aorta and (b) small mesenteric arteries from control, AngII-infused, or AngII + HsTX[R14A]-infused mice. Representative traces of ACh responses are also shown. (c) KCNA3 mRNA expression in cultured human microvascular endothelial cells incubated with AngII ($1 \text{ nmol} \cdot \text{L}^{-1}$) at different time points. Results are presented as means \pm SEM; the numbers of animals in each group are shown in parentheses. * $P < .05$, significantly different from control; # $P < .05$, significantly different from AngII; one-way (c) or two-way ANOVA (a,b) followed by Bonferroni's post hoc test

in the aorta, which was also impaired by AngII (Figure S2B). In agreement with the results found with ACh, treatment with HsTX[R14A] prevented AngII-induced endothelial dysfunction (Figure S2B). Neither HsTX[R14A] nor [EWSS]ShK modified ACh-, DEA-NO-, or bradykinin-induced relaxation in the aorta or small mesenteric arteries from control mice (data not shown). These

findings revealed a new role of $K_{v1.3}$ channels in endothelial dysfunction induced by AngII.

ACh-induced relaxation is totally dependent on NO in the aorta, whereas in small mesenteric arteries, a combination of PGI_2 , NO, and EDHF is found (Ellis et al., 2003; Leung & Vanhoutte, 2017). On this basis, the beneficial effect of $K_{v1.3}$ blockers on aortic function could

TABLE 1 pD_2 ($-\log EC_{50}$) values of ACh and diethylamine NONOate (DEA-NO) in aorta and small mesenteric arteries (SMAs) from control, AngII-infused, or AngII + HsTX[R14A]-infused mice

		Aorta pD_2	SMA pD_2
Control	ACh	7.54 ± 0.21 (7)	6.86 ± 0.50 (8)
	DEA-NO	6.73 ± 0.22 (5)	7.75 ± 0.13 (7)
AngII	ACh	6.25 ± 0.34 (5)	6.74 ± 0.72 (7)
	DEA-NO	6.18 ± 0.25 (6)	7.43 ± 0.30 (8)
AngII + HsTX[R14A]	ACh	7.71 ± 0.18 (7)*	7.07 ± 0.69 (7)
	DEA-NO	6.65 ± 0.25 (7)	7.34 ± 0.25 (7)

Note: Data are expressed as mean ± SEM of the number of animals indicated in parentheses.

* $P < .05$, significantly different from AngII alone.

TABLE 2 pD_2 ($-\log EC_{50}$) values of ACh and diethylamine NONOate (DEA-NO) in aorta and from control, AngII-infused, or AngII + [EWSS]ShK-infused mice

		Aorta pD_2
Control	ACh	7.29 ± 0.67 (12)
	DEA-NO	6.76 ± 0.28 (5)
AngII	ACh	7.10 ± 1.52 (9)
	DEA-NO	6.17 ± 0.22 (7)
AngII + [EWSS]ShK	ACh	6.77 ± 1.55 (12)
	DEA-NO	6.30 ± 0.04 (6)

Note: Data are expressed as mean ± SEM of the number of animals indicated in parentheses.

be due to enhanced NO availability. We then evaluated the EDHF component of ACh-induced relaxation in segments of small mesenteric arteries treated with a combination of inhibitors of NOS (L-NAME) and COX (indomethacin). No differences in the EDHF component were observed between the control and AngII-infused mice (Figure S2C). However, this EDHF-mediated response was inhibited in the arteries of HsTX[R14A]-treated animals. These results suggest that the beneficial effects of HsTX[R14A] on endothelial function in mesenteric arteries could be due to enhanced NO, PGI_2 , or a combination of both.

We then evaluated the effect of AngII on endothelial $K_V1.3$ channels. We used cultured human microvascular endothelial cells exposed to AngII. These cells showed low *Kcna3* expression (Ct ~ 30) that was not modified by AngII incubation at any time point (Figure 2c), apparently excluding the role of endothelial $K_V1.3$ channels in AngII-induced endothelial dysfunction.

3.3 | Blockade of $K_V1.3$ channels does not affect VSMC electrophysiology

Next, we tested whether possible alterations in K_V currents in VSMCs might explain the effects of the $K_V1.3$ channel blockers on vascular

function. We recorded the total K_V currents in freshly isolated VSMCs from the aorta of control, AngII, and AngII + HsTX[R14A] animals. Figure 3a shows representative original traces of the total K_V currents recorded in freshly isolated myocytes from all experimental groups. We did not observe significant differences in the K_V current amplitude measured at the end of the 200-ms depolarizing pulses (Figure 3b). Accordingly, the resting membrane potential was similar among the three experimental groups (Figure 3c). Interestingly, cell capacitance, an indicator of membrane surface area, was significantly higher in VSMCs from AngII-infused animals than in control animals. Likewise, this increase was reversed in VSMCs from animals treated with HsTX [R14A] (Figure 3d).

To characterize the $K_V1.3$ channel current in terms of the total K_V current, the baseline K_V current was recorded in the presence and absence of HsTX[R14A] ($0.1 \text{ nmol} \cdot \text{L}^{-1}$). The selective $K_V1.3$ channel blocker induced a subtle reduction in K_V currents in all experimental groups, indicating a minor contribution of $K_V1.3$ channels to the total K_V current in VSMCs (Figure 3e). Thus, HsTX[R14A]-sensitive currents (Figure 3f) measured at -10 mV , which reflect the $K_V1.3$ channel component, were not significantly different between all cell types. Accordingly, the percentage of the inhibition of K_V current (Figure 3g) and the changes in membrane potential ($\Delta Em_{\text{Control}} = 1.2 \pm 1.4 \text{ mV}$, $\Delta Em_{\text{AngII}} = 1.9 \pm 2.6 \text{ mV}$, and $\Delta Em_{\text{AngII} + \text{HsTX[R14A]}} = 2.0 \pm 3.2 \text{ mV}$) induced by HsTX[R14A] treatment were similar in all experimental groups. These data indicate that the improvement of vascular function induced by chronic blockade of $K_V1.3$ channels is unrelated to changes in VSMC electrophysiology.

3.4 | AngII increases expression of $K_V1.3$ channels in perivascular adipose tissue and peritoneal macrophages

Potassium channels modulate macrophage physiology (Chandy et al., 2004). In addition, AngII increases macrophage infiltration in perivascular adipose tissue (Mikolajczyk & Guzik, 2019). We evaluated possible changes in the expression levels of $K_V1.3$ and $K_V1.5$ channels in macrophages. As shown in Figure 4a, AngII increased *Kcna3* mRNA expression in perivascular adipose tissue. Moreover, in peritoneal

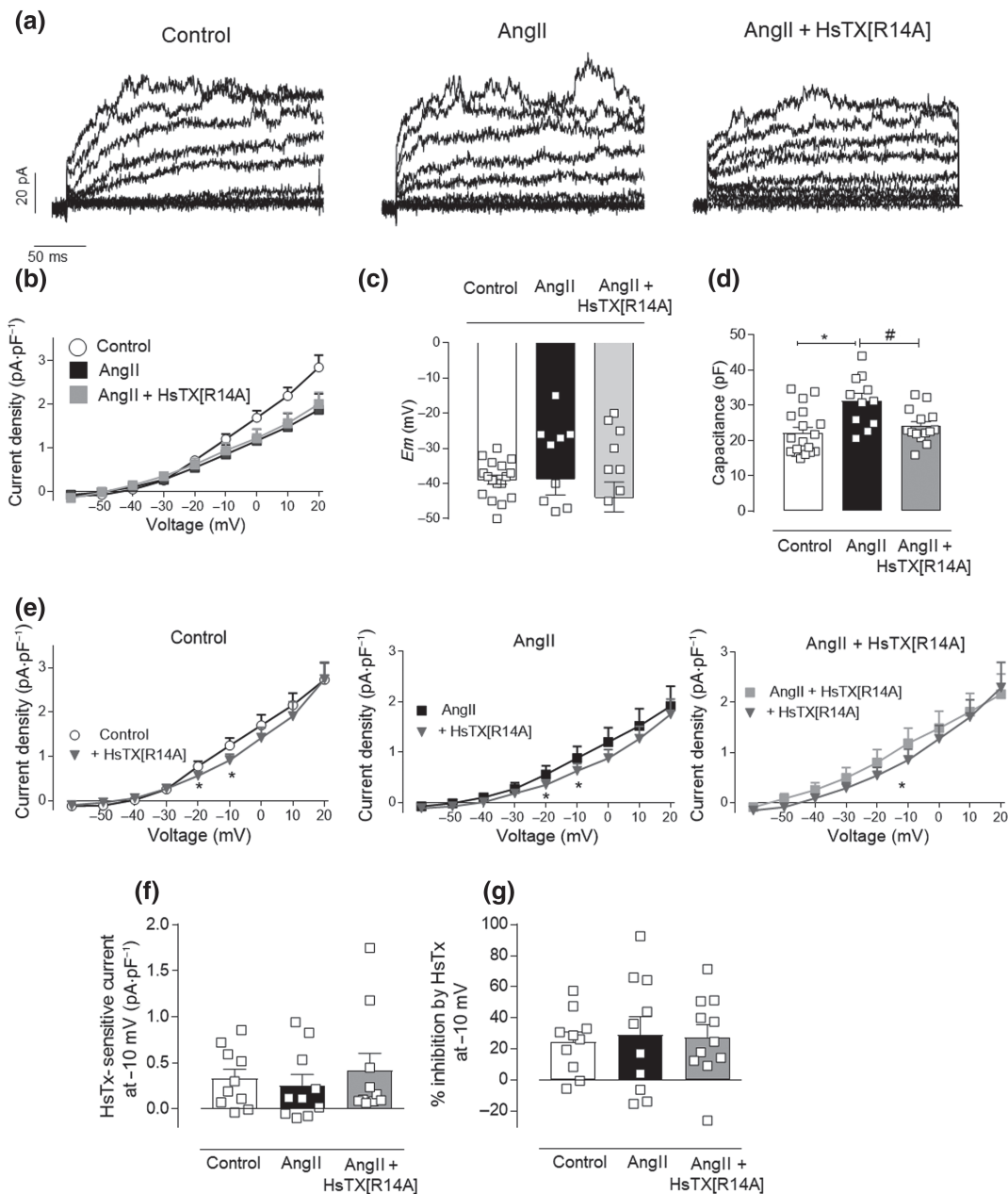


FIGURE 3 Improvement of vascular function by blocking $K_V1.3$ channels cannot be explained by changes in vascular smooth muscle cell (VSMC) electrophysiology. (a) Representative current traces for 200-ms depolarization pulses from -60 to +20 mV in 10-mV increments from a holding potential of -60 mV in VSMCs isolated from the aorta of control ($n = 18$), AngII-infused ($n = 11$) and AngII + HsTX[R14A]-infused ($n = 15$) mice (five animals per group). (b) Current-voltage relationships of K_V currents measured at the end of the pulse, analysed by a two-way ANOVA followed by Bonferroni's test. (c) Resting membrane potential (E_m) values in VSMC measured under current-clamp mode. (d) Average values of VSMC membrane capacitance. Both E_m and capacitance values were analysed using a one-way ANOVA followed by a Tukey's post hoc test ($n = 15$) from $n = 5$ treated mice from each group. (e) Current-voltage relationships of K_V currents measured at the end of the pulse before and after the addition of HsTX[R14A] in myocytes from control ($n = 10$), AngII-infused ($n = 10$), and AngII + HsTX[R14A]-infused ($n = 11$) mice, by a paired t test from $n = 5$ control or treated mice from each group. (f) HsTX[R14A]-sensitive current measured at -10 mV. (g) Percentage of inhibition of HsTX[R14A] measured at -10 mV. Results are presented as means \pm SEM for the number of experiments performed in VSMC obtained from five animals for each group. * $P < .05$, significantly different from control; # $P < .05$, significantly different from AngII; one-way ANOVA followed by Tukey's post hoc test

macrophages, AngII infusion markedly increased the protein and mRNA levels of $K_V1.3$ channels (Figure 4b,c) without affecting *Kcna5* mRNA expression; as a result, the *Kcna3/Kcna5* ratio was increased

by AngII (Figure 4c). Notably, HsTX[R14A] treatment completely blocked AngII-induced *Kcna3* expression without affecting *Kcna5* expression. Consequently, the *Kcna3/Kcna5* ratio was decreased by

HsTX[R14A] treatment (Figure 4c). HsTX[R14A] treatment did not modify *Kcna3* or *Kcna5* expression in control mice (data not shown). These results suggest a possible classical activation pathway of peritoneal macrophages in AngII-infused mice.

3.5 | Effects of AngII on the electrophysiological characteristics, cytokine profile, and infiltration of macrophages; effects of $K_V1.3$ channel blockade

AngII ($0.1 \mu\text{mol}\cdot\text{L}^{-1}$) perfused for 15–20 min on resting or LPS-activated peritoneal macrophages did not modify either the magnitude or the biophysical characteristics of the K_V currents

generated by the $K_V1.3/K_V1.5$ heterotetrameric channels (Figure S3), suggesting that AngII does not directly interact with $K_V1.3$ or $K_V1.5$ channels. However, the K_V current recorded in macrophages from AngII-infused mice exhibited an intermediate magnitude compared to those recorded from resting and LPS-induced M1 peritoneal macrophages (Figure S4). These results indicate that the effects observed in macrophages from AngII-infused mice could be due to changes in K_V channel expression, similar to those reported for macrophages incubated with LPS for 16 h (Moreno et al., 2013; Vicente et al., 2003).

In vitro addition of [EWSS]ShK ($1 \text{ nmol}\cdot\text{L}^{-1}$) or HsTX[R14A] ($0.1 \text{ nmol}\cdot\text{L}^{-1}$) inhibited the K_V current recorded in macrophages obtained from AngII-treated mice by $82.3 \pm 4.4\%$ ($n = 3$, exploratory results) and $93.3 \pm 1.6\%$ ($n = 3$, exploratory results), respectively. We

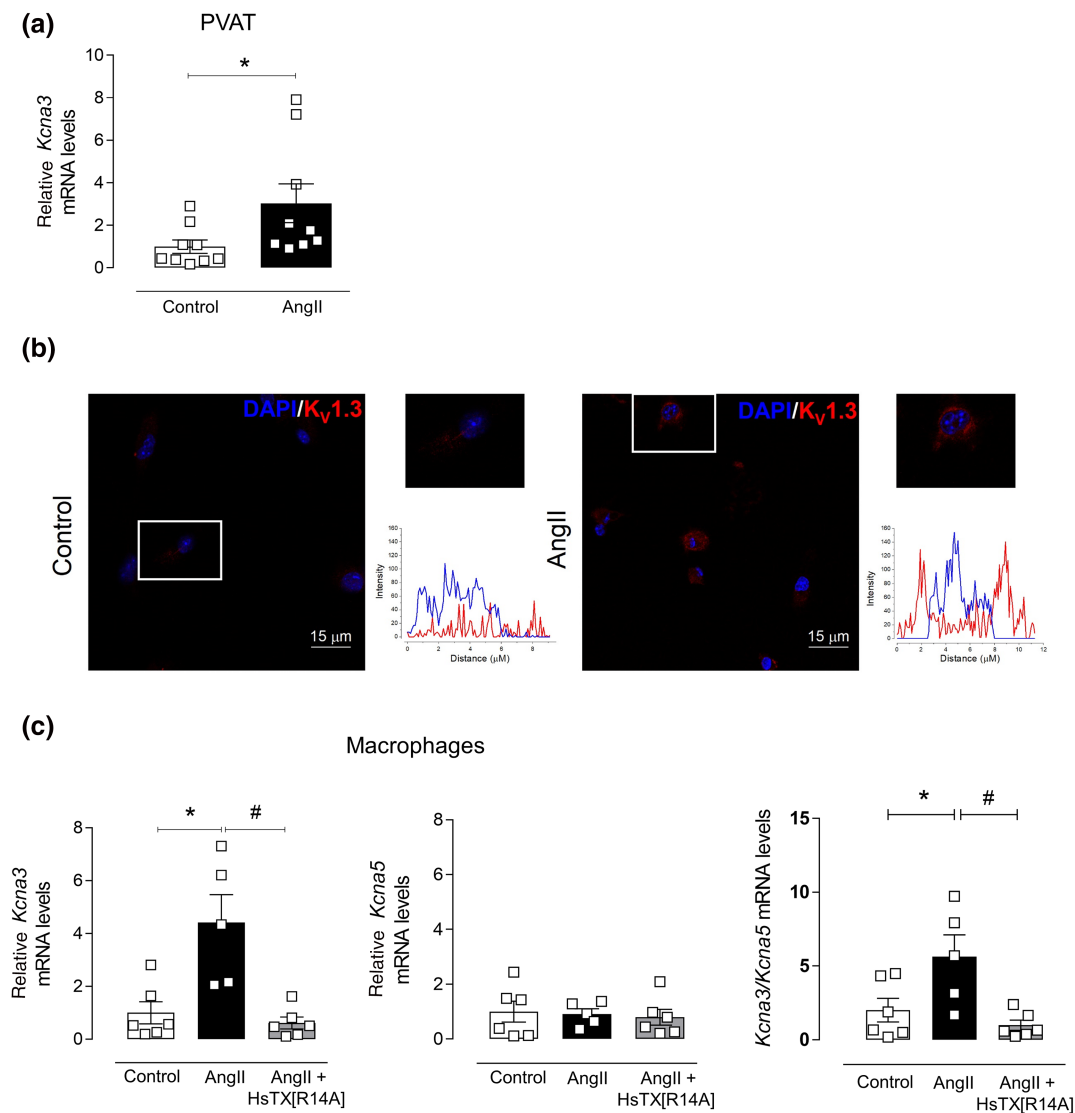


FIGURE 4 AngII increases expression of $K_V1.3$ channels in peritoneal macrophages and perivascular adipose tissue (PVAT). (a) *Kcna3* mRNA expression in PVAT from control and AngII animals ($n = 9$ for both groups). (b) Representative images of $K_V1.3$ protein expression in peritoneal macrophages from control ($n = 4$) and AngII ($n = 6$) animals. (c) *Kcna3* and *Kcna5* mRNA expression and the *Kcna3*/*Kcna5* ratio in peritoneal macrophages from control ($n = 6$), AngII ($n = 5$), and AngII + HsTX[R14A] mice ($n = 6$). Results are presented as means \pm SEM. * $P < .05$, significantly different from control; # $P < .05$, significantly different from AngII; Student's *t* test (a) or one-way ANOVA followed by Bonferroni's post hoc test (c)

then studied the biophysical characteristics of the K_V currents in peritoneal macrophages from control, AngII-, AngII + HsTX[R14A]-, and AngII + [EWSS]ShK-treated mice. As shown in Figure 5a,b, K_V currents recorded for macrophages from AngII-infused mice were greater than those recorded in macrophages obtained from the control group. More importantly, the electrophysiological characteristics of the K_V channels of macrophages from AngII-infused animals exhibited use-dependent effects (Figure 5c,d) and a greater degree of inactivation together with a faster time constant of inactivation (Figure 5e,f), similar to those exhibited by $K_V1.3$ channels (Chang et al., 2015; Moreno et al., 2013; Vicente et al., 2003; Villalonga et al., 2010). Treatment of AngII-infused mice with HsTX[R14A]

reversed these effects (Figure 5). Indeed, macrophages from AngII + HsTX[R14A] mice exhibited K_V currents similar to those generated by cells from control mice (Figure 5a–f). Similar effects were observed in peritoneal macrophages from AngII + [EWSS]ShK mice (Figure S5). Moreover, treatment of control mice with HsTX[R14A] or [EWSS]ShK did not modify the magnitude of the K_V current, the use dependency, or the percentage of inactivation of the K_V current (data not shown). Taken together, these results suggest that, like LPS, AngII treatment increases the $K_V1.3/K_V1.5$ ratio in the heterotetrameric channels present in peritoneal macrophages.

Subsequently, we evaluated the expression levels of M1 markers in macrophages from control, AngII, and AngII + HsTX[R14A] mice.

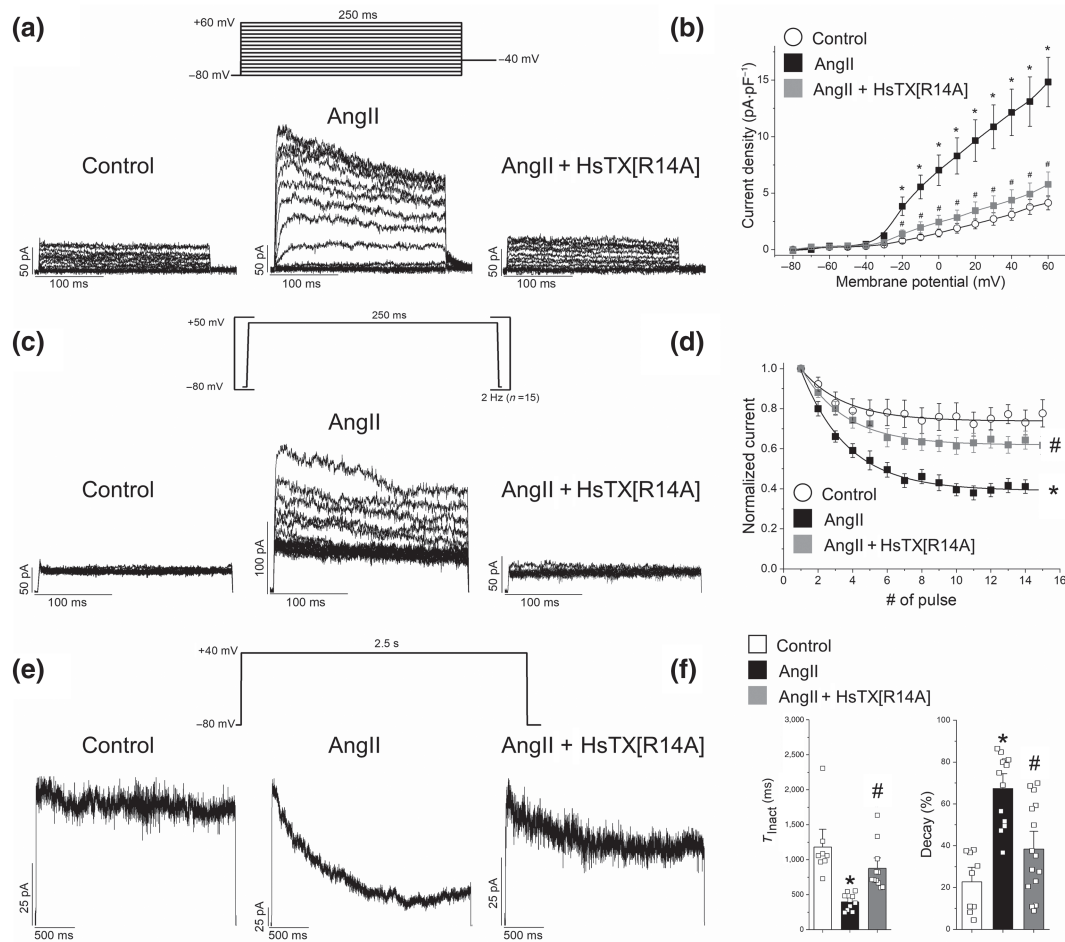


FIGURE 5 Blockade of $K_V1.3$ channels reverses the AngII-induced alterations in the electrophysiology of peritoneal macrophages.

(a) Representative current recordings obtained after applying 250-ms depolarizing pulses from -80 to $+60$ mV in 10-mV increments from a holding potential of -80 mV in peritoneal macrophages obtained from control ($n = 10$), AngII-infused ($n = 11$), and AngII + HsTX[R14A]-infused ($n = 27$) mice ($n = 5$ for each group). Tail currents were recorded after repolarizing to -40 mV. (b) Current-voltage relationships of K_V currents measured at the end of the 250-ms depolarizing pulses are shown in panel (a). (c) Cumulative K_V inactivation measured after applying trains of 15 pulses of 250 ms from -80 to $+50$ mV at 2 Hz in macrophages obtained from control ($n = 8$), AngII-infused ($n = 10$), and AngII + HsTX[R14A]-infused ($n = 20$) mice ($n = 5$ for each group). (d) Plots show the peak current amplitude at each pulse normalized to the peak current amplitude of the first pulse. Data were fitted to a mono-exponential function. (e) Current records obtained after applying a depolarizing pulse of 2.5 s from -80 to $+40$ mV in macrophages obtained from control ($n = 8$), AngII-infused ($n = 11$), and AngII + HsTX[R14A]-infused ($n = 11$) mice ($n = 5$ for each group). (f) Bars showing the time constant of inactivation (τ_{inact}) and the degree of pulse decay (%) for the long pulse shown in panel (e), as recorded in macrophages from control, AngII-infused, and AngII + HsTX[R14A]-infused mice ($n = 5$ for each group). Results are presented as means \pm SEM. * $P < .05$, significantly different from control; # $P < .05$, AngII + HsTX[R14A] significantly different from AngII; one-way ANOVA followed by Tukey's post hoc test

AngII significantly increased the expression of *Il6*, *Ptgs2*, and *Il1b* and did not modify the expression of *Tnfa* or *Cybb* (*Nox2*) (Figure 6a). Importantly, treatment with the $K_V1.3$ blocker HsTX[R14A] decreased the expression of *Ptgs2* and *Il1b* (Figure 6a). Moreover, AngII increased the expression of macrophage markers *Lamp2* (Mac-3) and *Adgre1* (F4/80) in perivascular adipose tissue, which was significantly reduced by HsTX[R14A] treatment (Figure 6b). However, neither AngII nor HsTX[R14A] modified macrophage content in the perivascular adipose tissue-denuded aorta (data not shown). HsTX [R14A] did not modify macrophage content in control mice (data not shown). Together, these data suggest that AngII infusion modifies macrophage infiltration and phenotype towards a more

proinflammatory phenotype and that treatment with a $K_V1.3$ channel blocker prevents these effects.

3.6 | Blockade of $K_V1.3$ channels prevents macrophage-induced endothelial dysfunction

Macrophages infiltrate the perivascular adventitia in arteries from AngII-infused mice and participate in endothelial dysfunction induced by AngII (De Ciuceis et al., 2005). Moreover, various studies, including ours, have demonstrated the role of COX-2 and IL-1 β in endothelial dysfunction (Jimenez-Altayo et al., 2006; Martinez-Revelles

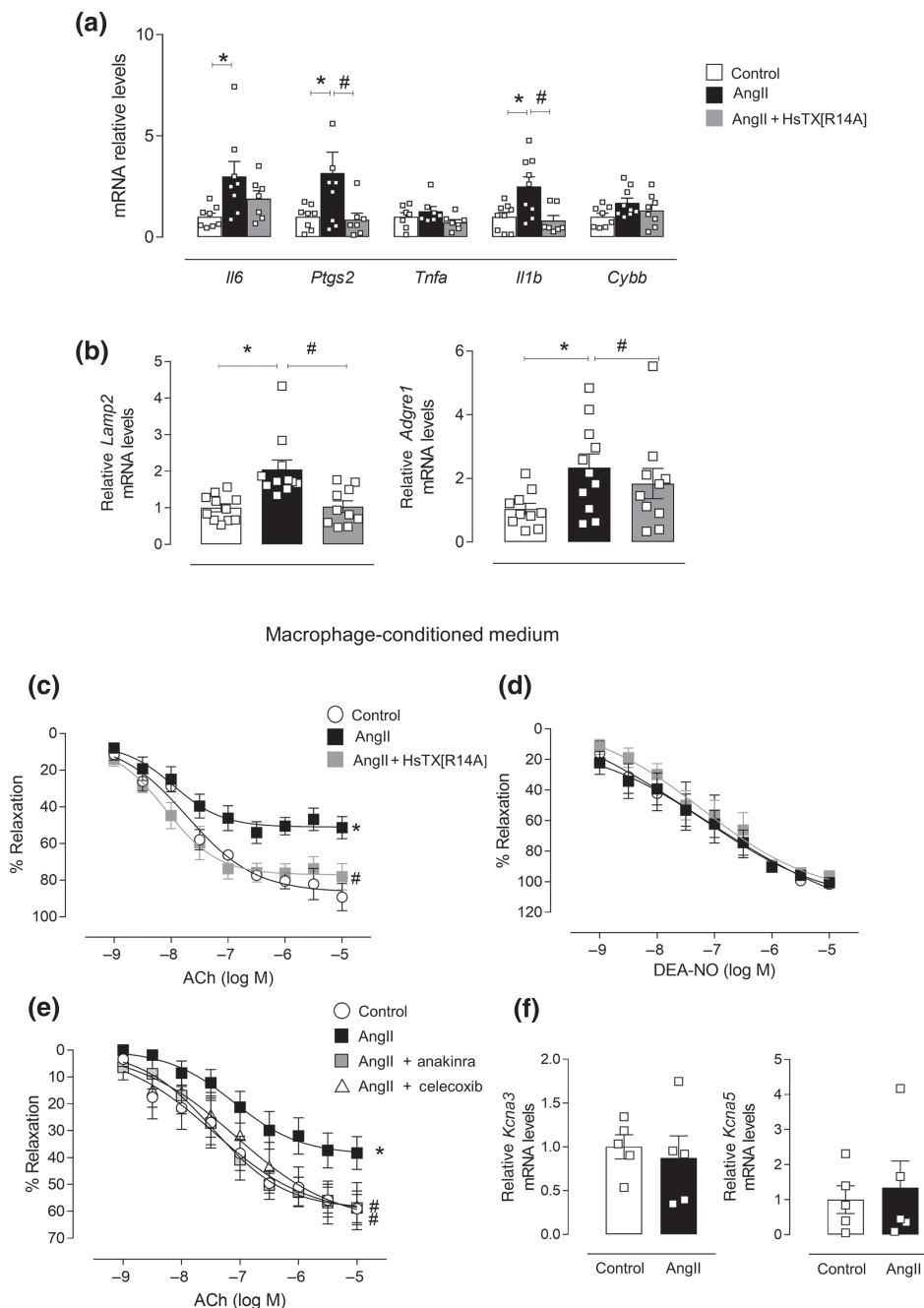


FIGURE 6 Blockade of $K_V1.3$ channels prevents macrophage-induced endothelial dysfunction in hypertension. (a) mRNA expression of M1 markers in peritoneal macrophages from control, AngII-infused, and AngII + HsTX[R14A]-infused mice. (b) mRNA expression of macrophage markers in perivascular adipose tissue from control, AngII-infused, and AngII + HsTX [R14A]-infused mice. Concentration-response curves to ACh (c) and diethylamine NONOate (DEA-NO) (d) in aorta from control animals incubated with macrophage-conditioned media from control ($n = 5$), AngII-infused ($n = 8$), and AngII + HsTX[R14A]-infused ($n = 7$) mice. (e) Concentration-response curves to ACh in aorta from control animals, incubated with macrophage-conditioned medium from control ($n = 6$) or AngII-infused animals ($n = 8$), in the presence or absence of anakinra ($100 \mu\text{g}\cdot\text{mL}^{-1}$) ($n = 8$) or celecoxib ($1 \mu\text{mol}\cdot\text{L}^{-1}$) ($n = 7$). (f) *Kcna3* and *Kcna5* mRNA expression in healthy aorta incubated for 20 h with macrophage-conditioned medium from control ($n = 5$) and AngII-infused ($n = 5$) mice. Results are presented as means \pm SEM. * $P < .05$, significantly different from control, # $P < .05$, significantly different from AngII; one-way (a,b) or two-way (c–e) ANOVA with Bonferroni's post hoc test; in (f), Student's *t* test

et al., 2013; Vallejo et al., 2014). We then raised the question whether the beneficial effect of systemic $K_V1.3$ channel blockade on endothelial function might be due to the modulation of macrophage phenotype.

To gain further insights into this, arteries from healthy untreated mice were incubated with macrophage-conditioned media from control, AngII, and AngII + HsTX[R14A] mice. Macrophage-conditioned media from AngII-infused mice, but not from control mice, significantly impaired aortic endothelium-dependent relaxation, and this effect was completely prevented in arteries incubated with AngII + HsTX[R14A] macrophage-conditioned media (Figure 6c, Table 3a). No differences in endothelium-independent relaxation were observed under the three experimental conditions (Figure 6d, Table 3a). Importantly, the endothelial dysfunction induced by macrophage-conditioned media from AngII-infused mice was also abolished by the IL-1 β blocker anakinra and by the selective COX-2 inhibitor celecoxib (Figure 6e, Table 3b). Neither anakinra nor celecoxib affected ACh-induced relaxation in arteries incubated with macrophage-conditioned media from control mice (data not shown). Interestingly, the expression of *Kcna3* and *Kcna5* in the aorta remained unaffected when incubated with macrophage-conditioned medium from control or AngII-infused mice (Figure 6f), further confirming the involvement of macrophage $K_V1.3$ in vascular function.

4 | DISCUSSION

Our study demonstrates for the first time that $K_V1.3$ channels play an important role in the macrophage-dependent endothelial dysfunction induced by AngII, most likely by facilitating macrophage infiltration in the surrounding perivascular adipose tissue and through modulation of the macrophage phenotype towards a proinflammatory M1-like phenotype.

Earlier evidence clearly suggested that increased expression of $K_V1.3$ channels and/or altered $K_V1.3/K_V1.5$ ratio made a significant contribution to the proliferation of VSMCs in several pathological conditions, such as neointima hyperplasia and endoluminal lesions (Cheong et al., 2011; Ciudad et al., 2010, 2014; Perez-Garcia et al., 2018). We found that AngII infusion increased $K_V1.3$ channel expression in the aorta, which was inhibited by HsTX[R14A]. However, we did not observe changes in vascular structure after treatment with $K_V1.3$ channel blockers, either in conductance or in resistance arteries from AngII-infused mice, most likely because this model is not associated with increased number of VSMCs (Briones, Rodriguez-Criado, et al., 2009; Hernanz et al., 2015), as compared with proliferative models of neointima hyperplasia. Nevertheless, HsTX[R14A] clearly reduced cell capacitance (a marker of cell surface area) in VSMCs from AngII-infused animals, indicating some anti-hypertrophic effect of the toxin that did not produce a clear contribution to the whole vessel structure. Importantly, the two selective $K_V1.3$ channel blockers completely prevented AngII-induced endothelial dysfunction, probably due to an increase in NO and/or PGI₂ availability, uncovering an unexpected role of these channels in

TABLE 3 (a) pD_2 ($-\log EC_{50}$) values of ACh and diethylamine NONOate (DEA-NO) in aorta from control animals incubated with macrophage-conditioned medium from control, AngII-infused, or AngII + HsTX[R14A]-infused mice, and (b) pD_2 values of ACh in aorta from control animals incubated with macrophage-conditioned medium from control or AngII animals plus anakinra (100 $\mu\text{g}\cdot\text{ml}^{-1}$) or celecoxib (1 μM)

		Aorta pD_2
(a)		
Control	ACh	7.69 \pm 0.19 (5)
	DEA-NO	7.27 \pm 0.56 (3)
AngII	ACh	7.93 \pm 0.30 (8)
	DEA-NO	7.26 \pm 0.37 (6)
AngII + HsTX[R14A]	ACh	8.12 \pm 0.12 (7)
	DEA-NO	7.03 \pm 0.36 (6)
(b)		
Control medium	ACh	7.51 \pm 0.29 (6)
AngII medium	ACh	6.90 \pm 0.31 (8)
AngII medium + anakinra	ACh	7.39 \pm 0.20 (8)
AngII medium + celecoxib	ACh	7.12 \pm 0.30 (7)

Note: Data are expressed as mean \pm SEM of the number of animals indicated in parentheses.

vascular function. In this context, an inhibition of relaxation rather than an improved endothelial function would have been expected, given the well-known effect of the inhibition of K^+ channels, which causes membrane depolarization and subsequent vasoconstriction (Cogolludo & Perez-Vizcaino, 2010; Jackson, 2018; Nelson & Quayle, 1995). Importantly, data from the electrophysiological studies discounted altered $K_V1.3$ currents in VSMCs as responsible for the beneficial effects of $K_V1.3$ channel blockade in AngII-induced endothelial dysfunction, suggesting that additional mechanisms were involved. In support, earlier studies had shown similar $K_V1.3$ channel expression in VSMC from a spontaneously hypertensive mouse model BPH (BP High), compared with their normotensive counterparts (Ciudad et al., 2014). Moreover, the presence of $K_V1.3$ channels in endothelial cells is controversial, although one study has reported $K_V1.3$ channel expression in rat brain endothelial cells (Millar et al., 2008). Further, we found low levels of $K_V1.3$ channels in a cell line of human endothelial cells, and expression of these channels was not affected by AngII.

Potassium channels play a critical role in maintaining the electrochemical gradient required for sustained Ca^{2+} entry in the timeframe necessary for activation and effects of macrophage functions. The K^+ currents generated in macrophages are due to the activation of the $K_V1.3/K_V1.5$ heterotetrameric channels (Moreno et al., 2013; Vicente et al., 2003; Villalonga et al., 2010). Blockade of $K_V1.3$ channels suppresses antigen-driven proliferation and cytokine production in T cells and macrophages. Therefore, selective $K_V1.3$ channel blockers ameliorate different pathologies that involve inflammation including multiple

sclerosis, autoimmune diabetes and acute liver injury (Beeton et al., 2005; Beeton, Barbaria, et al., 2001; Beeton, Wulff, et al., 2001; Chi et al., 2012; Rus et al., 2005; Wu et al., 2020). Our study demonstrates that $K_{V1.3}$ channels are important determinants of macrophage phenotype in AngII-induced hypertension, which in turn participates in endothelial dysfunction. Thus, in AngII-infused mice, expression of $K_{V1.3}$ channels increased in perivascular adipose tissue, an important site of macrophage accumulation. Moreover, $K_{V1.3}$ channel expression and the $K_{V1.3}/K_{V1.5}$ ratio, but not $K_{V1.5}$ expression, also increased in peritoneal macrophages probably due to either an increase in the $K_{V1.3}/K_{V1.5}$ ratio of heterotetramer channels, as described for the activation of macrophages with LPS, or by an increase in the homotetramers of $K_{V1.3}$ channels, suggesting an M1-like macrophage phenotype. Importantly, these changes in the expression pattern of $K_{V1.3}$ channels were abolished by HsTX[R14A] treatment. The effect of chronic AngII exposure on macrophage electrophysiology was not reproduced by acute administration, and short-term AngII administration did not modify LPS-induced biophysical properties either, suggesting that long-term adaptation processes, including increased expression of $K_{V1.3}$ channels, are needed to change the macrophage phenotype. We also found increased infiltration of macrophages in the perivascular adipose tissue in response to AngII infusion. Moreover, peritoneal macrophages obtained from AngII-treated mice exhibited an M1-like phenotype, as shown by the presence of enhanced M1 markers (IL-1 β , IL-6, and COX-2) and electrophysiological properties similar to those of LPS-stimulated macrophages, but clearly of smaller magnitude. In agreement, Wenzel et al. (2011) demonstrated that infusion of AngII for 7 days increased the expression of different proinflammatory genes, such as COX-2 or **NADPH oxidase NOX-2**, whereas other reports also showed enhanced M1 markers in vascular tissues from mice infused with AngII for 2 (Qian et al., 2014) and 4 weeks (Qi et al., 2019; Ye et al., 2019). However, M2-like macrophages were also found within the vascular wall after AngII infusion (Moore et al., 2015). Importantly, treatment of AngII-infused mice with selective blockers of $K_{V1.3}$ channels not only restored the altered electrophysiological properties of macrophages but also decreased excessive infiltration in perivascular adipose tissue and production of some proinflammatory markers, such as COX-2 and IL-1 β , suggesting decreased activation of M1-like macrophages by $K_{V1.3}$ channel blockade. This change in macrophage phenotype seems to have vascular functional consequences as we identified COX-2-derived products and IL-1 β released from AngII-activated macrophages to be responsible for macrophage-induced endothelial dysfunction. More importantly, macrophage-conditioned media from AngII + HsTX[R14A] mice did not affect vascular endothelial function, compared with the endothelial dysfunction induced by AngII-treated macrophages, thus supporting the role of macrophage $K_{V1.3}$ channels in endothelial dysfunction. In agreement, mRNA levels of either $K_{V1.3}$ or $K_{V1.5}$ did not change in aortic segments incubated with macrophage-conditioned media from control or AngII-infused mice. On the other hand, we cannot discard a modulatory role of $K_{V1.3}$ channels in AngII-induced ROS generation or an increase in **eNOS** activation as additional underlying

mechanisms involved in the improved endothelial function induced by $K_{V1.3}$ channel blockers.

A causal role for monocytes and macrophages in the development of hypertension, vascular remodelling, and endothelial dysfunction has been demonstrated in mice deficient in **macrophage colony-stimulating factor**, which renders them deficient in macrophages (De Ciuceis et al., 2005; Ko et al., 2007), and after selective ablation of lysozyme M-positive (LysM(+)) myelomonocytic cells by low-dose diphtheria toxin in mice with inducible expression of the **diphtheria toxin receptor** (LysM(iDTR) mice) (Kossmann et al., 2014; Wenzel et al., 2011). Our studies with macrophage-conditioned media agree with these reports and demonstrate the beneficial effect of $K_{V1.3}$ channel blockade in preventing macrophage-induced endothelial dysfunction in hypertension. However, none of the $K_{V1.3}$ blockers used in this study affected BP, in contrast to previous reports that used different approaches to inhibit macrophage presence (De Ciuceis et al., 2005; Ko et al., 2007; Moore et al., 2015; Wenzel et al., 2011). Of note, none of these highly selective compounds produced apparent off-targets effects either in macrophages or in the vasculature in control mice at the doses used here. One possible explanation for the lack of effect on BP might be that we found correction of endothelial dysfunction, but not vascular remodelling and stiffness. Although highly beneficial, this effect might not be sufficient to decrease BP. In addition, the role of $K_{V1.3}$ channels in other organs involved in BP control cannot be ruled out. In any case, our results demonstrate that the improvement in endothelial function, and macrophage infiltration and phenotype that occurs after $K_{V1.3}$ channel blockade is not merely a consequence of modified arterial pressure.

A limitation of our study is that we have analysed peritoneal macrophages instead of (peri)vascular macrophages and further studies are needed to confirm the increased expression of $K_{V1.3}$ channels and altered electrophysiology in this cell type. However, the fact that $K_{V1.3}$ expression was significantly increased by AngII in perivascular adipose tissue, which is rich in M1/M2 macrophages (Mikolajczyk et al., 2016), and was restored after $K_{V1.3}$ channel blockade partly supports experiments performed with peritoneal macrophages. In addition, peritoneal macrophages can migrate to adjacent tissues during inflammation (Cassado Ados et al., 2015), and despite their functional characteristics, they have been widely used as models for the activation of other types of tissue-resident macrophages, especially vascular macrophages. In this context, peritoneal macrophages have been used as models to study the behaviour of vascular macrophages in atherosclerosis or aortic aneurysms (Nakao et al., 2017). Moreover, peritoneal macrophages have been found to infiltrate atherosclerotic plaques as well (Sakai et al., 2018).

In summary, our results demonstrate that AngII increased the expression of $K_{V1.3}$ channels in the aorta, perivascular adipose tissue and macrophages. The increased expression of $K_{V1.3}$ channels and the altered biophysical properties observed in peritoneal macrophages suggests an M1-like activation in response to AngII. Blockade of $K_{V1.3}$ channels decreased the enhanced macrophage infiltration and the production of COX-2-derived products and proinflammatory cytokines, such as IL-1 β from macrophages, thus improving endothelial

function, without affecting vascular remodelling or BP. In conclusion, our study identified $K_v1.3$ channels as novel mediators of macrophage-dependent endothelial dysfunction in hypertension. $K_v1.3$ blockers are potential candidates for the treatment of not only autoimmune but also of vascular diseases.

ACKNOWLEDGEMENTS

This work was funded by the Ministerio de Economía y Competitividad; AEI-FEDER, EU grants: SAF2016-75021-R and PID2019-104366RB-C21 (to C.V.), SAF2016-80305-P (to A.M.B. and M.S.), and SAF2016-77222-R (to A.C.); Instituto de Salud Carlos III CIBERCV program: CB16/11/00286 (to M.S.) and CB/11/00222 (to C.V.); Consejo Superior de Investigaciones Científicas grants: PIE 201820E104 and 2019AEP148 (to C.V.) and Comunidad de Madrid grant: B2017/BMD-3676-AORTASANA (to M.S.) and B2017/BMD-3727 (to A.C.) with funds co-financed by ERDF (FEDER) Funds from the European Commission, "A way of making Europe"; and Comunidad de Madrid-Universidad Autónoma de Madrid grant: SI1-PJ1-2019-00321 (to A.B.G.-R.). The authors thank Drs Lisardo Boscá, Christine Beeton, and Raymond Norton for their helpful suggestions and Astrid Enero her help with some experiments.

AUTHOR CONTRIBUTIONS

A.B.A. and C.V. conceived and designed the research. M.A.O., M.M.-C., D.A.P., R.H., A.B.G.-R., and G.M.-P. performed experiments. M.A.O., M.M.-C., D.A.P., R.H., A.B.G.-R., G.M.-P., A.C., A.B.A., and C.V. analysed data and interpreted the results of the experiments. A.B.A. and C.V. drafted the manuscript. A.B.A., C.V., A.B.G.-R., M.S., and A.C. edited and revised the manuscript. All authors approved the final version of the manuscript.

CONFLICT OF INTEREST

M.W.P. was the CEO of Peptides International and was involved in design and synthesis of the two patented $K_v1.3$ channel blocking peptides used in this study. The other authors report no conflicts.

DECLARATION OF TRANSPARENCY AND SCIENTIFIC RIGOUR

This Declaration acknowledges that this paper adheres to the principles for transparent reporting and scientific rigour of preclinical research as stated in the *BJP* guidelines for [Design & Analysis](#), [Immunoblotting and Immunochemistry](#), and [Animal Experimentation](#), and as recommended by funding agencies, publishers, and other organizations engaged with supporting research.

DATA AVAILABILITY STATEMENT

The data supporting the findings of this study are available from the corresponding authors upon reasonable request. Some data may not be made available because of privacy or ethical restrictions.

ORCID

Miguel A. Olivencia  <https://orcid.org/0000-0002-9563-8191>

Ana B. García-Redondo  <https://orcid.org/0000-0002-5815-3320>

Angel Cogolludo  <https://orcid.org/0000-0002-1382-1698>

Ana M. Briones  <https://orcid.org/0000-0001-8218-5579>

REFERENCES

- Alexander, S. P. H., Fabbro, D., Kelly, E., Mathie, A., Peters, J. A., Veale, E. L., Armstrong, J. F., Faccenda, E., Harding, S. D., Pawson, A. J., Sharman, J. L., Southan, C., Davies, J. A., & CGTP Collaborators. (2019). THE CONCISE GUIDE TO PHARMACOLOGY 2019/20: Enzymes. *British Journal of Pharmacology*, 176, S297–S396. <https://doi.org/10.1111/bph.14752>
- Alexander, S. P. H., Mathie, A., Peters, J. A., Veale, E. L., Striessnig, J., Kelly, E., Armstrong, J. F., Faccenda, E., Harding, S. D., Pawson, A. J., Sharman, J. L., Southan, C., Davies, J. A., & CGTP Collaborators. (2019). THE CONCISE GUIDE TO PHARMACOLOGY 2019/20: Ion channels. *British Journal of Pharmacology*, 176, S142–S228. <https://doi.org/10.1111/bph.14749>
- Alexander, S. P. H., Roberts, R. E., Broughton, B. R. S., Sobey, C. G., George, C. H., Stanford, S. C., Cirino, G., Docherty, J. R., Giembycz, M. A., Hoyer, D., Insel, P. A., Izzo, A. A., Ji, Y., MacEwan, D. J., Mangum, J., Wonnacott, S., & Ahluwalia, A. (2018). Goals and practicalities of immunoblotting and immunohistochemistry: A guide for submission to the *British Journal of Pharmacology*. *British Journal of Pharmacology*, 175, 407–411. <https://doi.org/10.1111/bph.14112>
- Beeton, C., Barbaria, J., Giraud, P., Devaux, J., Benoliel, A. M., Gola, M., Sabatier, J. M., Bernard, D., Crest, M., & Beraud, E. (2001). Selective blocking of voltage-gated K^+ channels improves experimental autoimmune encephalomyelitis and inhibits T cell activation. *Journal of Immunology*, 166, 936–944. <https://doi.org/10.4049/jimmunol.166.2.936>
- Beeton, C., Pennington, M. W., Wulff, H., Singh, S., Nugent, D., Crossley, G., Khaytin, I., Calabresi, P. A., Chen, C. Y., Gutman, G. A., & Chandy, K. G. (2005). Targeting effector memory T cells with a selective peptide inhibitor of $K_v1.3$ channels for therapy of autoimmune diseases. *Molecular Pharmacology*, 67, 1369–1381. <https://doi.org/10.1124/mol.104.008193>
- Beeton, C., Wulff, H., Barbaria, J., Clot-Faybesse, O., Pennington, M., Bernard, D., Cahalan, M. D., Chandy, K. G., & Beraud, E. (2001). Selective blockade of T lymphocyte K^+ channels ameliorates experimental autoimmune encephalomyelitis, a model for multiple sclerosis. *Proceedings of the National Academy of Sciences of the United States of America*, 98, 13942–13947. <https://doi.org/10.1073/pnas.241497298>
- Bergmann, R., Kubeil, M., Zarschler, K., Chhabra, S., Tajhya, R. B., Beeton, C., Pennington, M. W., Bachmann, M., Norton, R. S., & Stephan, H. (2017). Distribution and kinetics of the $K_v1.3$ -blocking peptide HsTX1[R14A] in experimental rats. *Scientific Reports*, 7, 3756. <https://doi.org/10.1038/s41598-017-03998-x>
- Bobi, J., Garabito, M., Solanes, N., Ciudad, P., Ramos-Perez, V., Ponce, A., Rigol, M., Freixa, X., Pérez-Martínez, C., de Prado, A. P., Fernández-Vázquez, F., Sabaté, M., Borrós, S., López-López, J. R., Pérez-García, M. T., & Roque, M. (2020). $K_v1.3$ blockade inhibits proliferation of vascular smooth muscle cells in vitro and intimal hyperplasia in vivo. *Translational Research*, 224, 40–54. <https://doi.org/10.1016/j.trsl.2020.06.002>
- Briones, A. M., Gonzalez, J. M., Somoza, B., Giraldo, J., Daly, C. J., Vila, E., Carmen González, M., McGrath, J. C., & Arribas, S. M. (2003). Role of elastin in spontaneously hypertensive rat small mesenteric artery remodelling. *The Journal of Physiology*, 552, 185–195. <https://doi.org/10.1113/jphysiol.2003.046904>
- Briones, A. M., Padilha, A. S., Cogolludo, A. L., Alonso, M. J., Vassallo, D. V., Perez-Vizcaino, F., & Salaices, M. (2009). Activation of BKCa channels by nitric oxide prevents coronary artery endothelial dysfunction in ouabain-induced hypertensive rats. *Journal of Hypertension*, 27, 83–91. <https://doi.org/10.1097/HJH.0b013e328317a7cf>

- Briones, A. M., Rodriguez-Criado, N., Hernanz, R., Garcia-Redondo, A. B., Rodrigues-Diez, R. R., Alonso, M. J., Egido, J., Ruiz-Ortega, M., & Salaices, M. (2009). Atorvastatin prevents angiotensin II-induced vascular remodeling and oxidative stress. *Hypertension*, *54*, 142–149. <https://doi.org/10.1161/HYPERTENSIONAHA.109.133710>
- Caillon, A., Paradis, P., & Schiffrin, E. L. (2019). Role of immune cells in hypertension. *British Journal of Pharmacology*, *176*, 1818–1828. <https://doi.org/10.1111/bph.14427>
- Cassado Ados, A., D'Imperio Lima, M. R., & Bortoluci, K. R. (2015). Revisiting mouse peritoneal macrophages: Heterogeneity, development, and function. *Frontiers in Immunology*, *6*, 225.
- Chandy, K. G., Wulff, H., Beeton, C., Pennington, M., Gutman, G. A., & Cahalan, M. D. (2004). K⁺ channels as targets for specific immunomodulation. *Trends in Pharmacological Sciences*, *25*, 280–289. <https://doi.org/10.1016/j.tips.2004.03.010>
- Chang, S. C., Huq, R., Chhabra, S., Beeton, C., Pennington, M. W., Smith, B. J., & Norton, R. S. (2015). N-terminally extended analogues of the K⁺ channel toxin from *Stichodactyla helianthus* as potent and selective blockers of the voltage-gated potassium channel Kv1.3. *The FEBS Journal*, *282*, 2247–2259. <https://doi.org/10.1111/febs.13294>
- Cheong, A., Li, J., Sukumar, P., Kumar, B., Zeng, F., Riches, K., Munsch, C., Wood, I. C., Porter, K. E., & Beech, D. J. (2011). Potent suppression of vascular smooth muscle cell migration and human neointimal hyperplasia by K_v1.3 channel blockers. *Cardiovascular Research*, *89*, 282–289. <https://doi.org/10.1093/cvr/cvq305>
- Chi, V., Pennington, M. W., Norton, R. S., Tarcha, E. J., Londono, L. M., Sims-Fahey, B., Upadhyay, S. K., Lakey, J. T., Iadonato, S., Wulff, H., Beeton, C., & Chandy, K. G. (2012). Development of a sea anemone toxin as an immunomodulator for therapy of autoimmune diseases. *Toxicol*, *59*, 529–546. <https://doi.org/10.1016/j.toxicol.2011.07.016>
- Cidad, P., Moreno-Dominguez, A., Novensa, L., Roque, M., Barquin, L., Heras, M., Pérez-García, M. T., & Lopez-Lopez, J. R. (2010). Characterization of ion channels involved in the proliferative response of femoral artery smooth muscle cells. *Arteriosclerosis, Thrombosis, and Vascular Biology*, *30*, 1203–1211. <https://doi.org/10.1161/ATVBAHA.110.205187>
- Cidad, P., Novensa, L., Garabito, M., Battle, M., Dantas, A. P., Heras, M., López-López, J. R., Pérez-García, M. T., & Roque, M. (2014). K⁺ channels expression in hypertension after arterial injury, and effect of selective Kv1.3 blockade with PAP-1 on intimal hyperplasia formation. *Cardiovascular Drugs and Therapy*, *28*, 501–511. <https://doi.org/10.1007/s10557-014-6554-5>
- Clement-Chomienne, O., Ishii, K., Walsh, M. P., & Cole, W. C. (1999). Identification, cloning and expression of rabbit vascular smooth muscle Kv1.5 and comparison with native delayed rectifier K⁺ current. *The Journal of Physiology*, *515*(Pt 3), 653–667. <https://doi.org/10.1111/j.1469-7793.1999.653ab.x>
- Cogolludo, A., Moreno, L., Lodi, F., Frazziano, G., Cobeno, L., Tamargo, J., & Perez-Vizcaino, F. (2006). Serotonin inhibits voltage-gated K⁺ currents in pulmonary artery smooth muscle cells: Role of 5-HT_{2A} receptors, caveolin-1, and Kv1.5 channel internalization. *Circulation Research*, *98*, 931–938. <https://doi.org/10.1161/01.RES.0000216858.04599.e1>
- Cogolludo, A., & Perez-Vizcaino, F. (2010). 5-HT receptors and K_v channel internalization. *Advances in Experimental Medicine and Biology*, *661*, 391–401. https://doi.org/10.1007/978-1-60761-500-2_25
- Curtis, M. J., Alexander, S., Cirino, G., Docherty, J. R., George, C. H., Giembycz, M. A., Hoyer, D., Insel, P. A., Izzo, A. A., Ji, Y., MacEwan, D. J., Sobey, C. G., Stanford, S. C., Teixeira, M. M., Wonnacott, S., & Ahluwalia, A. (2018). Experimental design and analysis and their reporting II: Updated and simplified guidance for authors and peer reviewers. *British Journal of Pharmacology*, *175*, 987–993. <https://doi.org/10.1111/bph.14153>
- De Ciuceis, C., Amiri, F., Brassard, P., Endemann, D. H., Touyz, R. M., & Schiffrin, E. L. (2005). Reduced vascular remodeling, endothelial dysfunction, and oxidative stress in resistance arteries of angiotensin II-infused macrophage colony-stimulating factor-deficient mice: Evidence for a role in inflammation in angiotensin-induced vascular injury. *Arteriosclerosis, Thrombosis, and Vascular Biology*, *25*, 2106–2113. <https://doi.org/10.1161/01.ATV.0000181743.28028.57>
- Drummond, G. R., Vinh, A., Guzik, T. J., & Sobey, C. G. (2019). Immune mechanisms of hypertension. *Nature Reviews. Immunology*, *19*, 517–532. <https://doi.org/10.1038/s41577-019-0160-5>
- Ellis, A., Pannirselvam, M., Anderson, T. J., & Triggle, C. R. (2003). Catalase has negligible inhibitory effects on endothelium-dependent relaxations in mouse isolated aorta and small mesenteric artery. *British Journal of Pharmacology*, *140*, 1193–1200. <https://doi.org/10.1038/sj.bjp.0705549>
- Hernanz, R., Martinez-Revelles, S., Palacios, R., Martin, A., Cachofeiro, V., Aguado, A., Garcia-Redondo, L., Barrús, M. T., De Batista, P. R., Briones, A. M., Salaices, M., & Alonso, M. J. (2015). Toll-like receptor 4 contributes to vascular remodelling and endothelial dysfunction in angiotensin II-induced hypertension. *British Journal of Pharmacology*, *172*, 3159–3176. <https://doi.org/10.1111/bph.13117>
- Jackson, W. F. (2018). K_v channels and the regulation of vascular smooth muscle tone. *Microcirculation*, *25*, e12421. <https://doi.org/10.1111/micc.12421>
- Jimenez-Altayo, F., Briones, A. M., Giraldo, J., Planas, A. M., Salaices, M., & Vila, E. (2006). Increased superoxide anion production by interleukin-1 β impairs nitric oxide-mediated relaxation in resistance arteries. *The Journal of Pharmacology and Experimental Therapeutics*, *316*, 42–52. <https://doi.org/10.1124/jpet.105.088435>
- Khemili, D., Valenzuela, C., Laraba-Djebari, F., & Hammoudi-Triki, D. (2019). Differential effect of *Androctonus australis hector* venom components on macrophage K_v channels: Electrophysiological characterization. *European Biophysics Journal*, *48*, 1–13. <https://doi.org/10.1007/s00249-018-1323-1>
- Ko, E. A., Amiri, F., Pandey, N. R., Javeshghani, D., Leibovitz, E., Touyz, R. M., Schiffrin, E., & L. (2007). Resistance artery remodeling in deoxycorticosterone acetate-salt hypertension is dependent on vascular inflammation: Evidence from m-CSF-deficient mice. *American Journal of Physiology. Heart and Circulatory Physiology*, *292*, H1789–H1795. <https://doi.org/10.1152/ajpheart.01118.2006>
- Kossmann, S., Hu, H., Steven, S., Schonfelder, T., Fraccarollo, D., Mikhed, Y., Brähler, M., Knorr, M., Brandt, M., Karbach, S. H., & Wenzel, P. (2014). Inflammatory monocytes determine endothelial nitric-oxide synthase uncoupling and nitro-oxidative stress induced by angiotensin II. *The Journal of Biological Chemistry*, *289*, 27540–27550. <https://doi.org/10.1074/jbc.M114.604231>
- Lerman, L. O., Kurtz, T. W., Touyz, R. M., Ellison, D. H., Chade, A. R., Crowley, S. D., Mattson, D. L., Mullins, J. J., Osborn, J., Eirin, A., Reckelhoff, J. F., Iadecola, C., & Coffman, T. (2019). Animal models of hypertension: A scientific statement from the American Heart Association. *Hypertension*, *73*, e87–e120. <https://doi.org/10.1161/HYP.000000000000090>
- Leung, S. W., & Vanhoutte, P. M. (2017). Endothelium-dependent hyperpolarization: Age, gender and blood pressure, do they matter? *Acta Physiologica (Oxford, England)*, *219*, 108–123. <https://doi.org/10.1111/apha.12628>
- Lilley, E., Stanford, S. C., Kendall, D. E., Alexander, S. P., Cirino, G., Docherty, J. R., George, C. H., Insel, P. A., Izzo, A. A., Ji, Y., Panettieri, R. A., Sobey, C. G., Stefanska, B., Stephens, G., Teixeira, M., & Ahluwalia, A. (2020). ARRIVE 2.0 and the *British Journal of Pharmacology*: Updated guidance for 2020. *British Journal of Pharmacology*, *177*(16), 3611–3616. <https://bpspubs.onlinelibrary.wiley.com/doi/full/10.1111/bph.15178>
- Martinez-Revelles, S., Avendaño, M. S., Garcia-Redondo, A. B., Alvarez, Y., Aguado, A., Perez-Giron, J. V., García-Redondo, L., Esteban, V.,

- Redondo, J. M., Alonso, M. J., Briones, A. M., & Salaices, M. (2013). Reciprocal relationship between reactive oxygen species and cyclooxygenase-2 and vascular dysfunction in hypertension. *Antioxidants & Redox Signaling*, *18*, 51–65. <https://doi.org/10.1089/ars.2011.4335>
- Mikolajczyk, T. P., & Guzik, T. J. (2019). Adaptive immunity in hypertension. *Current Hypertension Reports*, *21*, 68. <https://doi.org/10.1007/s11906-019-0971-6>
- Mikolajczyk, T. P., Nosalski, R., Szczepaniak, P., Budzyn, K., Osmenda, G., Skiba, D., Sagan, A., Wu, J., Vinh, A., Marvar, P. J., Guzik, B., Podolec, J., Drummond, G., Lob, H. E., Harrison, D. G., & Guzik, T. J. (2016). Role of chemokine RANTES in the regulation of perivascular inflammation, T-cell accumulation, and vascular dysfunction in hypertension. *The FASEB Journal*, *30*, 1987–1999. <https://doi.org/10.1096/fj.201500088R>
- Millar, I. D., Wang, S., Brown, P. D., Barrand, M. A., & Hladky, S. B. (2008). Kv1 and Kir2 potassium channels are expressed in rat brain endothelial cells. *Pflügers Archiv*, *456*, 379–391. <https://doi.org/10.1007/s00424-007-0377-1>
- Moore, J. P., Vinh, A., Tuck, K. L., Sakkal, S., Krishnan, S. M., Chan, C. T., Lieu, M., Samuel, C. S., Diep, H., Kemp-Harper, B. K., Tare, M., Ricardo, S. D., Guzik, T. J., Sobey, C. G., & Drummond, G. R. (2015). M2 macrophage accumulation in the aortic wall during angiotensin II infusion in mice is associated with fibrosis, elastin loss, and elevated blood pressure. *American Journal of Physiology. Heart and Circulatory Physiology*, *309*, H906–H917. <https://doi.org/10.1152/ajpheart.00821.2014>
- Moreno, C., Prieto, P., Macías, A., Pimentel-Santillana, M., de la Cruz, A., Traves, P. G., Boscá, L., & Valenzuela, C. (2013). Modulation of voltage-dependent and inward rectifier potassium channels by 15-epi-lipoxin-A4 in activated murine macrophages: Implications in innate immunity. *Journal of Immunology*, *191*, 6136–6146. <https://doi.org/10.4049/jimmunol.1300235>
- Nakao, T., Horie, T., Baba, O., Nishiga, M., Nishino, T., Izuhara, M., Kuwabara, Y., Nishi, H., Usami, S., Nakazeki, F., Ide, Y., & Ono, K. (2017). Genetic ablation of microRNA-33 attenuates inflammation and abdominal aortic aneurysm formation via several anti-inflammatory pathways. *Arteriosclerosis, Thrombosis, and Vascular Biology*, *37*, 2161–2170. <https://doi.org/10.1161/ATVBAHA.117.309768>
- Nelson, M. T., & Quayle, J. M. (1995). Physiological roles and properties of potassium channels in arterial smooth muscle. *The American Journal of Physiology*, *268*, C799–C822. <https://doi.org/10.1152/ajpcell.1995.268.4.C799>
- Norlander, A. E., Madhur, M. S., & Harrison, D. G. (2018). The immunology of hypertension. *The Journal of Experimental Medicine*, *215*, 21–33. <https://doi.org/10.1084/jem.20171773>
- Percie du Sert, N., Hurst, V., Ahluwalia, A., Alam, S., Avey, M. T., Baker, M., Browne, W. J., Clark, A., Cuthill, I. C., Dirnagl, U., Emerson, M., Garner, P., Holgate, S. T., Howells, D. W., Karp, N. A., Lazic, S. E., Lidster, K., MacCallum, C. J., Macleod, M., ... Würbel, H. (2020). The ARRIVE guidelines 2.0: Updated guidelines for reporting animal research. *PLoS Biology*, *18*(7), e3000410. <https://doi.org/10.1371/journal.pbio.3000410>
- Perez-Garcia, M. T., Ciudad, P., & Lopez-Lopez, J. R. (2018). The secret life of ion channels: Kv1.3 potassium channels and proliferation. *American Journal of Physiology. Cell Physiology*, *314*, C27–C42. <https://doi.org/10.1152/ajpcell.00136.2017>
- Qi, D., Wei, M., Jiao, S., Song, Y., Wang, X., Xie, G., Taranto, J., Liu, Y., Duan, Y., Yu, B., Li, H., Shah, Y. M., Xu, Q., du, J., Gonzalez, F. J., & Qu, A. (2019). Hypoxia inducible factor 1 α in vascular smooth muscle cells promotes angiotensin II-induced vascular remodeling via activation of CCL7-mediated macrophage recruitment. *Cell Death & Disease*, *10*, 544. <https://doi.org/10.1038/s41419-019-1757-0>
- Qian, L., Li, X., Fang, R., Wang, Z., Xu, Y., Zhang, H., Bai, H., Yang, Q., Zhu, X., Ben, J., Xu, Y., & Chen, Q. (2014). Class A scavenger receptor deficiency augments angiotensin II-induced vascular remodeling. *Biochemical Pharmacology*, *90*, 254–264. <https://doi.org/10.1016/j.bcp.2014.05.015>
- Rashid, M. H., Huq, R., Tanner, M. R., Chhabra, S., Khoo, K. K., Estrada, R., Dhawan, V., Chauhan, S., Pennington, M. W., Beeton, C., Kuyucak, S., & Norton, R. S. (2014). A potent and Kv1.3-selective analogue of the scorpion toxin HsTX1 as a potential therapeutic for autoimmune diseases. *Scientific Reports*, *4*, 4509.
- Rus, H., Pardo, C. A., Hu, L., Darrah, E., Cudrici, C., Niculescu, T., Niculescu, F., Mullen, K. M., Allie, R., Guo, L., Wulff, H., Beeton, C., Judge, S. I. V., Kerr, D. A., Knaus, H. G., Chandy, K. G., & Calabresi, P. A. (2005). The voltage-gated potassium channel Kv1.3 is highly expressed on inflammatory infiltrates in multiple sclerosis brain. *Proceedings of the National Academy of Sciences of the United States of America*, *102*, 11094–11099. <https://doi.org/10.1073/pnas.0501770102>
- Sakai, K., Nagashima, S., Wakabayashi, T., Tumenbayar, B., Hayakawa, H., Hayakawa, M., Karasawa, T., Ohashi, K., Yamazaki, H., Takei, A., Takei, S., Yamamuro, D., Takahashi, M., Yagyu, H., Osuga, J. I., Takahashi, M., Tominaga, S. I., & Ishibashi, S. (2018). Myeloid HMG-CoA (3-hydroxy-3-methylglutaryl-coenzyme A) reductase determines atherosclerosis by modulating migration of macrophages. *Arteriosclerosis, Thrombosis, and Vascular Biology*, *38*, 2590–2600. <https://doi.org/10.1161/ATVBAHA.118.311664>
- Tanner, M. R., Tajhya, R. B., Huq, R., Gehrmann, E. J., Rodarte, K. E., Atik, M. A., Norton, R. S., Pennington, M. W., & Beeton, C. (2017). Prolonged immunomodulation in inflammatory arthritis using the selective Kv1.3 channel blocker HsTX1[R14A] and its PEGylated analog. *Clinical Immunology*, *180*, 45–57. <https://doi.org/10.1016/j.clim.2017.03.014>
- Upadhyay, S. K., Eckel-Mahan, K. L., Mirbolooki, M. R., Tjong, I., Griffey, S. M., Schmunk, G., Koehne, A., Halbout, B., Iadonato, S., Pedersen, B., Borrelli, E., Wang, P. H., Mukherjee, J., Sassone-Corsi, P., & Chandy, G. (2013). Selective Kv1.3 channel blocker as therapeutic for obesity and insulin resistance. *Proceedings of the National Academy of Sciences of the United States of America*, *110*, E2239–E2248. <https://doi.org/10.1073/pnas.1221206110>
- Vallejo, S., Palacios, E., Romacho, T., Villalobos, L., Peiro, C., & Sanchez-Ferrer, C. F. (2014). The interleukin-1 receptor antagonist anakinra improves endothelial dysfunction in streptozotocin-induced diabetic rats. *Cardiovascular Diabetology*, *13*, 158. <https://doi.org/10.1186/s12933-014-0158-z>
- Vicente, R., Escalada, A., Coma, M., Fuster, G., Sanchez-Tillo, E., Lopez-Iglesias, C., Soler, C., Solsona, C., Celada, A., & Felipe, A. (2003). Differential voltage-dependent K⁺ channel responses during proliferation and activation in macrophages. *The Journal of Biological Chemistry*, *278*, 46307–46320. <https://doi.org/10.1074/jbc.M304388200>
- Vicente, R., Escalada, A., Villalonga, N., Texido, L., Roura-Ferrer, M., Martin-Satue, M., López-Iglesias, C., Soler, C., Solsona, C., Tamkun, M. M., & Felipe, A. (2006). Association of Kv1.5 and Kv1.3 contributes to the major voltage-dependent K⁺ channel in macrophages. *The Journal of Biological Chemistry*, *281*, 37675–37685. <https://doi.org/10.1074/jbc.M605617200>
- Villalonga, N., David, M., Bielanska, J., Vicente, R., Comes, N., Valenzuela, C., & Felipe, A. (2010). Immunomodulation of voltage-dependent K⁺ channels in macrophages: Molecular and biophysical consequences. *The Journal of General Physiology*, *135*, 135–147. <https://doi.org/10.1085/jgp.200910334>
- Wenzel, P., Knorr, M., Kossmann, S., Stratmann, J., Hausding, M., Schuhmacher, S., Karbach, S. H., Schwenk, M., Yogeve, N., Schulz, E., Celze, M., & Munzel, T. (2011). Lysozyme M-positive monocytes mediate angiotensin II-induced arterial hypertension and vascular dysfunction. *Circulation*, *124*, 1370–1381. <https://doi.org/10.1161/CIRCULATIONAHA.111.034470>



- Wu, B., Liu, J. D., Bian, E., Hu, W., Huang, C., Meng, X., Zhang, L., Lv, X., & Li, J. (2020). Blockage of Kv1.3 regulates macrophage migration in acute liver injury by targeting δ -catenin through RhoA signaling. *International Journal of Biological Sciences*, 16, 671–681. <https://doi.org/10.7150/ijbs.38950>
- Ye, J., Que, B., Huang, Y., Lin, Y., Chen, J., Liu, L., Shi, Y., Wang, Y., Wang, M., Zeng, T., Wang, Z., Hu, H., Xu, Y., Shi, L., Ye, D., Liu, J., Jiang, H., Wan, J., & Ji, Q. (2019). Interleukin-12p35 knockout promotes macrophage differentiation, aggravates vascular dysfunction, and elevates blood pressure in angiotensin II-infused mice. *Cardiovascular Research*, 115, 1102–1113. <https://doi.org/10.1093/cvr/cvy263>
- Zhang, X., Goncalves, R., & Mosser, D. M. (2008). The isolation and characterization of murine macrophages. *Current Protocols in Immunology*, 83, 14–11. Chapter 14: Unit 14 11

SUPPORTING INFORMATION

Additional supporting information may be found online in the Supporting Information section at the end of this article.

How to cite this article: Olivencia MA, Martínez-Casales M, Peraza DA, et al. Kv1.3 channels are novel determinants of macrophage-dependent endothelial dysfunction in angiotensin II-induced hypertension in mice. *Br J Pharmacol*. 2021;178: 1836–1854. <https://doi.org/10.1111/bph.15407>